REPORT NVL-0059-009

(1) LEVEL III

A066918

AD A074457

STUDY OF ELECTRONIC TRANSPORT AND BREAKDOWN IN THIN INSULATING FILMS

Walter C. Johnson
PRINCETON UNIVERSITY
Department of Electrical Engineering
and Computer Science
Princeton, New Jersey 08540
Telephone: (609) 452-4621

1 December 1978

SEMI-ANNUAL TECHNICAL REPORT NO. 6

Approved for public release; distribution unlimited.

DDC FILE COPY

Prepared for:

NIGHT VISION AND ELECTO-OPTICS LABORATORIES
U. S. Army Electronics Command
Fort Belvoir, Virginia 22060

DDC
RECEIVED
OCT 1 1979
B

Sponsored by:

DEFENSE ADVANCED RESEARCH PROJECTS AGENCY

DARPA Order No. 3466
Program Code No. Y10
Contract DAAG53-76-C-0059
Effective Date: 17 November 1975
Expiration Date: 30 September 1979

79 09 25 019

Unclassified

SECURITY CLASSIFICATION OF THIS PAGE (When Data Entered)

REPORT DOCUMENTATION PAGE		READ INSTRUCTIONS BEFORE COMPLETING FORM
1. REPORT NUMBER (18) NVL-0059-79 (19)	2. GOVT ACCESSION NO.	3. RECIPIENT'S CATALOG NUMBER
4. TITLE (and Subtitle) (6) STUDY OF ELECTRONIC TRANSPORT AND BREAKDOWN IN THIN INSULATING FILMS.		5. TYPE OF REPORT & PERIOD COVERED 6. PERFORMING ORG. REPORT NUMBER
7. AUTHOR(s) (10) Walter C. Johnson Telephone: (609) 452-4621		8. CONTRACT OR GRANT NUMBER(s) (15) DAAG53-76-C-0059, ARPA Order-3466
9. PERFORMING ORGANIZATION NAME AND ADDRESS Princeton University Department of Electrical Engineering Princeton, New Jersey 08540	400 734	10. PROGRAM ELEMENT, PROJECT, TASK AREA & WORK UNIT NUMBERS 62912E, ARPA 3466, Y10, 024CJ
11. CONTROLLING OFFICE NAME AND ADDRESS Defense Advanced Research Projects Agency (11) 1400 Wilson Boulevard Arlington, Virginia 22209		12. REPORT DATE 1 Dec [redacted] 78 13. NUMBER OF PAGES 86
14. MONITORING AGENCY NAME & ADDRESS (if different from Controlling Office) Night Vision & Electro-Optics Laboratories DELNV-EO Fort Belvoir, Virginia 22060		15. SECURITY CLASS. (of this report) Unclassified 15a. DECLASSIFICATION/DOWNGRADING SCHEDULE

16. DISTRIBUTION STATEMENT (of this Report)

Approved for public release; distribution unlimited

(12) 87

17. DISTRIBUTION STATEMENT (of the abstract entered in Block 20, if different from Report)

(9) Semi-annual technical rept. no. 6

18. SUPPLEMENTARY NOTES

19. KEY WORDS (Continue on reverse side if necessary and identify by block number)

Insulating Films
Electronic Transport in Insulators
Charge Trapping in Insulators
Dielectric Breakdown
Silicon Dioxide
Silicon nitride
Aluminum oxide

20. ABSTRACT (Continue on reverse side if necessary and identify by block number)

Recent progress is reported in an ongoing program of sutdies of high-field effects in thin insulating films on semiconducting substrates. The investigations reported here include further studies of the high-field generation of interface states in the Si-SiO_2 system, a comparison between the effects of ionizing radiation and high-field stress in generating interface states in MOS capacitors, and a study of the characteristics of charge trapping in CVD Al_2O_3 on silicon

400 734

DD FORM 1 JAN 73 1473 EDITION OF 1 NOV 65 IS OBSOLETE
S/N 0102-014-6601

Unclassified

SECURITY CLASSIFICATION OF THIS PAGE (When Data Entered)

TABLE OF CONTENTS

1. INTRODUCTION

We report here on recent progress in an ongoing program of research directed toward a basic understanding of the electronic properties of thin insulating films and of the interfaces of such films with semiconductors and metals. Of particular interest are the high-field properties, including charge-carrier injection through the interfaces, electronic transport through the insulator, charge-carrier trapping and recombination at the interfaces and in the insulator, the high-field generation of interface states and trapping centers, and the mechanisms leading to dielectric breakdown. The objective of the program is to provide a rational basis for the choice of materials, processing methods and treatment of the insulating films in order to obtain the desired performance and reliability. The insulating films under study at the present time are silicon dioxide and aluminum oxide on silicon substrates. We have also studied silicon nitride and high-pressure-grown silicon dioxide. The techniques and apparatus that we have developed under this program are, moreover, immediately applicable to the study of other types of insulating films and substrates.

In Ch. 2 of this report, Genda Hu of our staff discusses the results obtained in his investigation of the high-field generation of interface states in the $Si-SiO_2$ system. The generation of interface states is inhibited at liquid nitrogen tempeterature. Following high-field stress at 90°K and warmup, the generation of states proceeds as $t^{1/4}$. He finds that the number of states generated in a fixed time is linearly proportional to the number of trapped holes in the oxide, and he observes that the straight line has a slope of 0.5 at 20°C and 0.85 at 66°C. A negative bias applied to the MOS capacitor while interface-state generation is taking place decreases the final number of interface states, while positive bias increases the number of generated states. The $t^{1/4}$ dependence and the effect of bias may indicate that diffusion of a negatively charged species away from the interface is involved. Photoinjection of electrons at 90°K produces some immediate generation of interface states but reduces the final number of states generated after warmup.

In Ch. 3, Genda Hu discusses the results of a comparison he has made between the interface states generated in the $Si-SiO_2$ system after high field stress and those generated after exposure of the MOS structure to ionizing radiation. Similar to the result mentioned in the preceding paragraph for high-field-generated interface states, the number of interface states generated in one hour after exposure to ionizing radiation is linearly proportional to the number of holes trapped in the oxide. He further compared the results of high field stress and of soft X-ray irradiation by observing the time evolution of the quasi-static C-V curves at successively higher temperatures. From these curves he calculated the energy distribution of the generated interface states. Both the time evolution of the C-V curves and the energy distribution of the interface states were remarkably similar after high-field stress and X-irradiation. These results provide convincing evidence that these two causes of interface-state generation operate in much the same way: they produce holes, some of which are trapped at or near the $Si-SiO_2$ interface, and the trapped holes are responsible for the formation of the interface states. The generation of the states is inhibited at liquid nitrogen temperature but proceeds for a long time after the sample is warmed to room temperature. If the sample is warmed above room temperature the generation of states proceeds more rapidly and the distribution in energy is progressively altered. Annealing of the interface states is eventually observed as the temperature is raised. This study is continuing.

In Ch. 4 of this report, S. S. Li presents the results of his investigation of charge trapping in thin films of CVD Al_2O_3 on silicon substrates. By use of photodepopulation, he finds both shallow (< 2.5 eV) and deep electron traps distributed through the bulk of the oxide. The concentration of traps is large, and when electrons are injected into the oxide many of them do not get all the way through the insulator but instead are trapped. Mr. Li presents an analysis of this, and he shows results which indicate that the capture cross section of the traps is of the order of 10^{-13} cm^2 and that the trap concentration is as high as 6×10^{18} cm^{-3}. His studies of the energy distribution of the trapped electrons and the position of the centroid

of the trapped charge indicate that the shallowly trapped electrons can be detrapped by a field-assisted, thermally activated process. Some of the detrapped electrons are subsequently retrapped more stably in deeper centers. The spatial profile of the trapped charge is thus dependent on temperature and on the applied field, and is affected by the space charge of the trapped electrons themselves.

2. A STUDY OF THE HIGH-FIELD GENERATION OF INTERFACE STATES IN MOS CAPACITORS

(Genda Hu collaborating)

2.1. Introduction

C. C. Chang[1] appears to have been the first to report that after an MOS capacitor had been stressed at a high electric field, no generation of interface states was observed if the sample was kept at low temperatures, but once the temperature was raised, interface states began to be generated. Later, J. J. Clement[2,3] and C. S. Jenq[3-8] not only confirmed this phenomenon but, in addition, found that low temperature inhibited the formation of interface states after exposure to X-rays. Jenq[4,6] developed a Low Temperature C-V Displacment (LTD) method for measuring the density of interface states within the central region of the bandgap at low temperature.

We have made a further study of the high-field generation of interface states. In this report we shall present a model to explain the continuous generation of interface states after warmup. Also, we shall comment on some resemblances between the generation of interface states at high fields after exposure to high fields and after exposure to ionizing radiation.

2.2. Samples

All of the samples used in these experiments had n-type (100) silicon substrates with 5-10 Ω-cm resistivity. The oxides were thermally grown in dry oxygen to a thickness of 1200Å. Each sample had an Aℓ gate which was about 120Å in thickness. This was thin enough to allow us to photoinject electrons and permitted the high-field breakdown of the oxide to be self-quenched.[9]

2.3. The Formation of Interface States at Room Temperature After High-Field Stress

Jenq[4] has reported that the generation of interface states continues for a considerable time after the high-field-stressed sample has been brought to room temperature. The same phenomenon was also observed by Winokur et al[10] after an MOS structure had been exposed to high energy radiation at room temperature.

We performed a set of experiments on some 30 samples. The high-field biasing was performed at liquid nitrogen temperature for 25 minutes. In order to avoid forming a deep depletion layer in the n-type substrate, only positive gate biases were used. The average field in the oxide ranged from 5.86 MV/cm to 7.73 MV/cm. After stressing, the sample was warmed to room temperature. The generation of interface states at room temperature was traced over a period of more than two months by occasionally cooling the sample to liquid nitrogen temperature and using the LTD method to measure the interface state density in the mid 0.7 eV region of the bandgap. The sample was then warmed to room temperature to allow the generation of interface states to proceed. Except when noted otherwise, a condition of zero bias was used during warmup. The effect of nonzero bias during warmup will be discussed in Sec. 2.5(B).

We found that the buildup of interface states, N_{ss} cm^{-2}, after the sample was brought to room temperature, was best described by the function t^n, where n is approximately 1/4. The number of interface states appeared to saturate. Figures 2.1 and 2.2 show plots of N_{ss} against $t^{1/4}$ for different stress fields. These results are similar to those obtained by C. S. Jenq[4] after high field stress and by Winokur et al[10] after exposure to ionizing radiation. In contrast with the good fit obtained by plotting against $t^{1/4}$, we show in Figs. 2.3 and 2.4 the unsatisfactory results obtained by plotting against the logarithm of time.

A $t^{1/4}$ dependence of the generation of interface states has also been found by Jeppson and Svensson[11] in an investigation of the negative-bias-stress (NBS) effect in MOS structures. Their MOS samples were stressed by electric fields from 4 MV/cm to 6 MV/cm at elevated temperature (25-125°C). They explained their results on the basis of a diffusion-controlled model and proposed that OH groups were the responsible diffusing species. A. G. Revesz[12] supported this model from the viewpoint of a chemist. Also, C. T. Sah[13] proposed a similar model in which OH^- ions drifted to the positive gate during the irradiation process. In order to get more insight into the mechanisms of interface-state generation, we

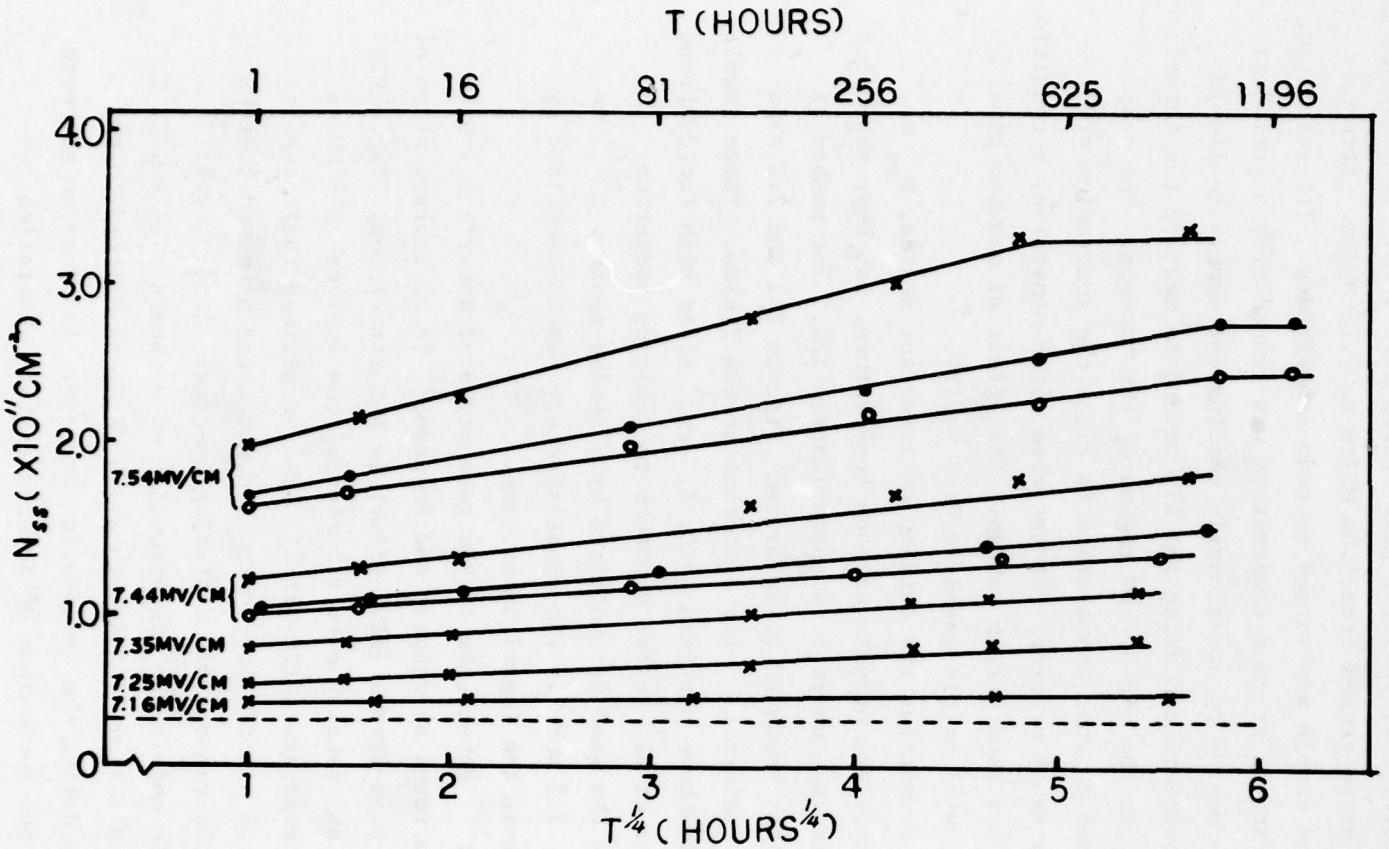

Fig. 2.1. N_{ss}, the density of interface states in room temperature after high-field stress for 25 minutes at 90°K, plotted against $(\text{time})^{1/4}$ with field strength as a parameter. The dotted line shows the interface states of a fresh sample.

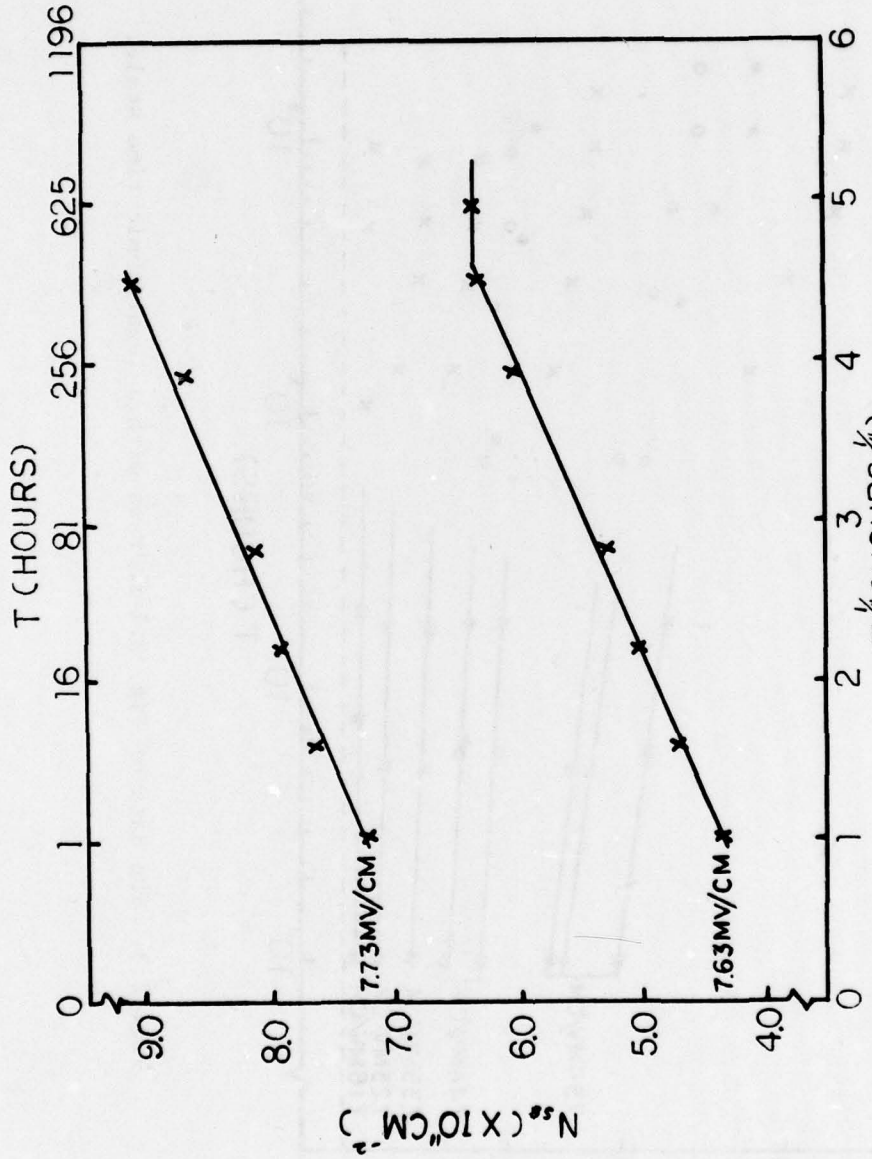

Fig. 2.2. Similar to Fig. 2.1, but for higher fields.

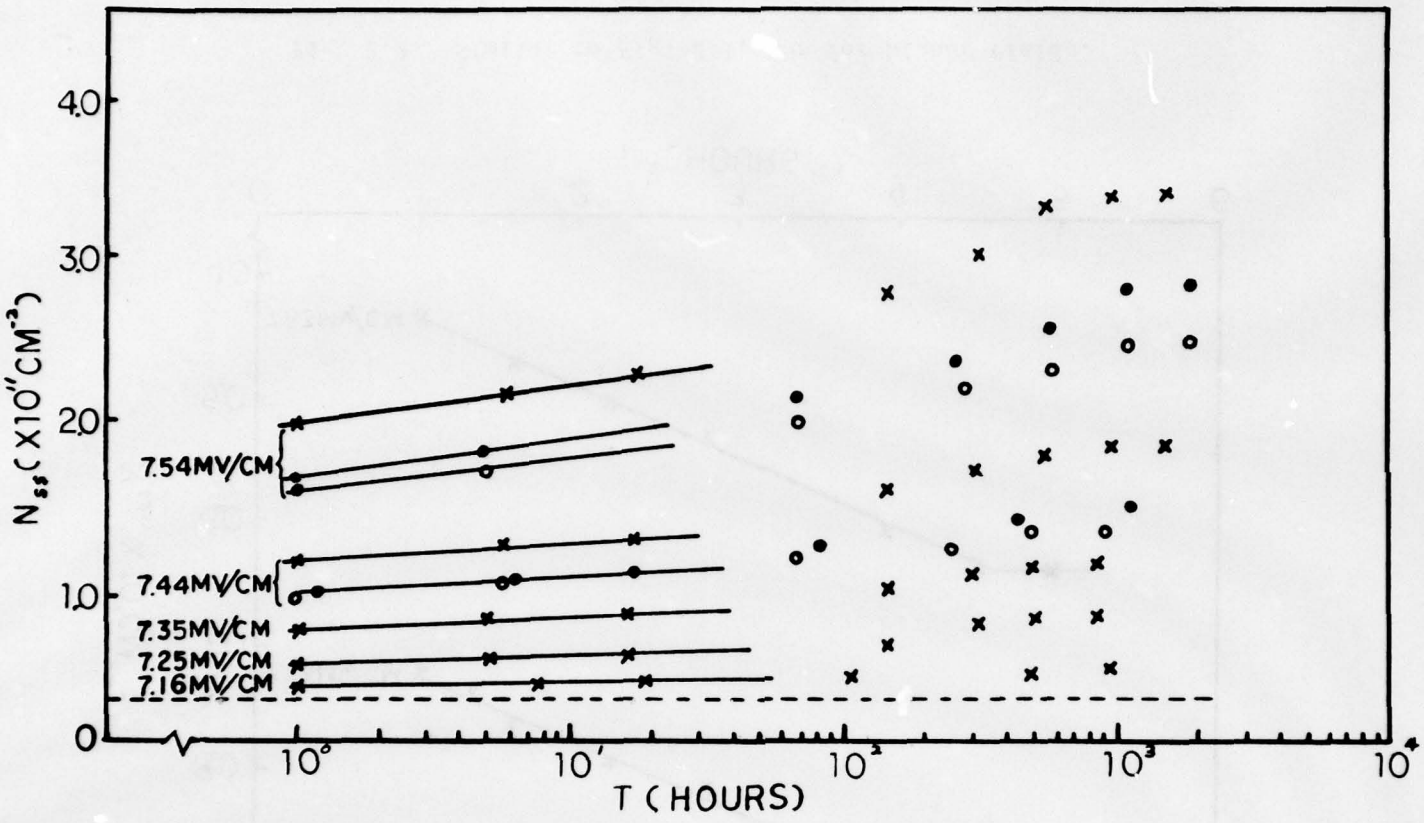

Fig. 2.3. The data of Fig. 2.1 redrawn with a logarithmic time scale.

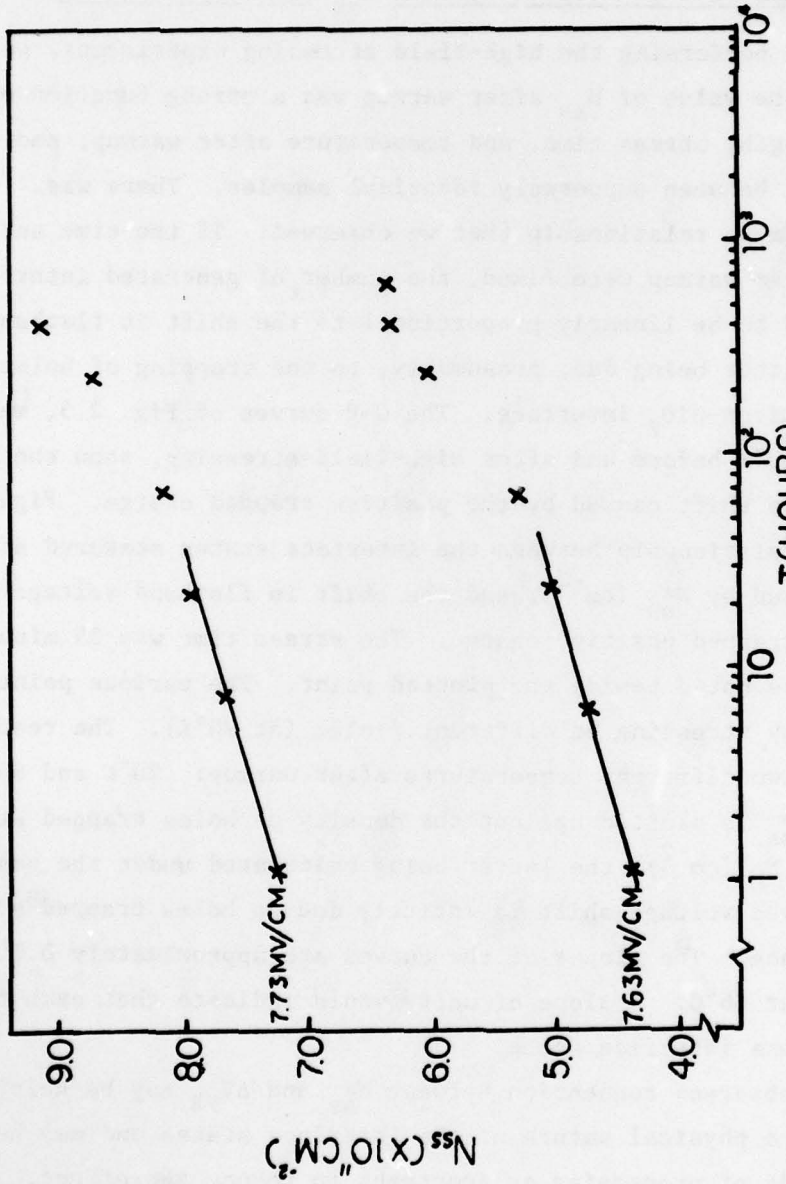

Fig. 2.4. The data of Fig. 2.2 redrawn with a logarithmic time scale.

examined the effects of temperature, the bias during the warmup period, and electron photoinjection in our experiments. The results will be presented in Section 2.5.

2.4. Observation of a Connection Between N_{ss} and Trapped Holes

While performing the high-field stressing experiments, we observed that the value of N_{ss} after warmup was a strong function of the field strength, stress time, and temperature after warmup, and varied somewhat between supposedly identical samples. There was, however, one simple relationship that we observed: If the time and temperature after warmup were fixed, the number of generated interface states appeared to be linearly proportional to the shift in flatband voltage, the latter being due, presumably, to the trapping of holes at or near the silicon-SiO_2 interface. The C-V curves of Fig. 2.5, which were taken at 90°K before and after high-field stressing, show the lateral negative shift caused by the positive trapped charge. Figure 2.6 shows the relationship between the interface states measured after one hour, denoted by N^*_{ss} (cm^{-2}), and the shift in flatband voltage caused by the trapped positive charge. The stress time was 25 minutes unless otherwise noted beside the plotted point. The various points were obtained by stressing at different fields (at 90°K). The results are shown for two different temperatures after warmup: 20°C and 66°C. In Fig. 2.7, N^*_{ss} is plotted against the density of holes trapped at the interface, N_h (cm^{-2}), the latter being calculated under the assumption that the observed voltage shift is entirely due to holes trapped at the Si-SiO_2 interface. The slopes of the curves are approximately 0.50 at 20°C and 0.85 at 66°C. A slope of unity would indicate that each trapped hole produced one interface state.

The observed connection between N^*_{ss} and ΔV_{FB} may be helpful in establishing the physical nature of the interface states and may help to indicate methods of processing or treatment to reduce the effect. In particular, the relationship indicates that radiation-hard MOS structures should also be electric-field-hard.

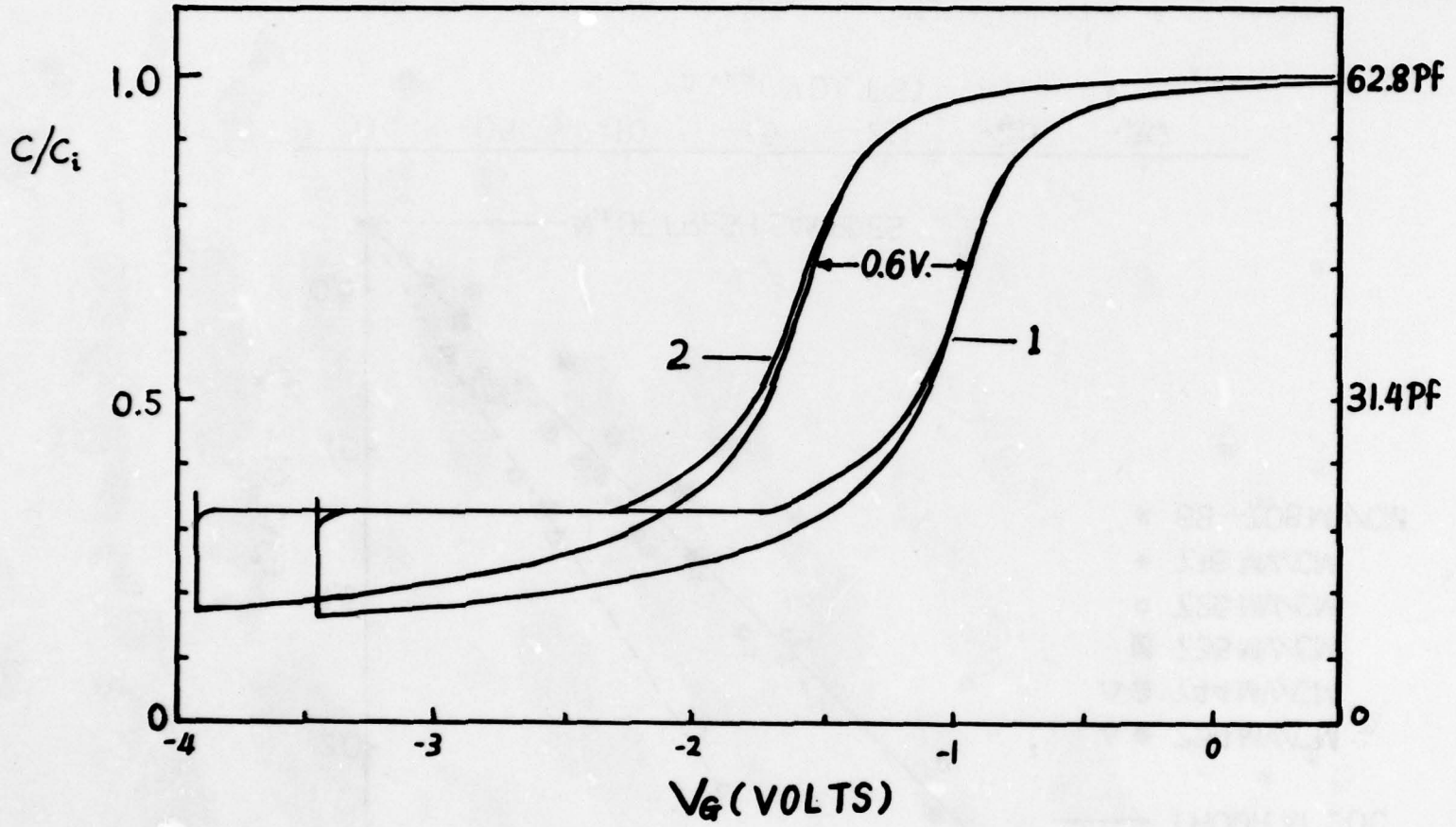

Fig. 2.5. Low temperature C-V curves taken at 90°K. (1) Before high-field stress. (2) After stressing at 7.44 MV/cm for 25 min. The shift from Curve 1 to Curve 2 shows the storage of positive charge in the oxide.

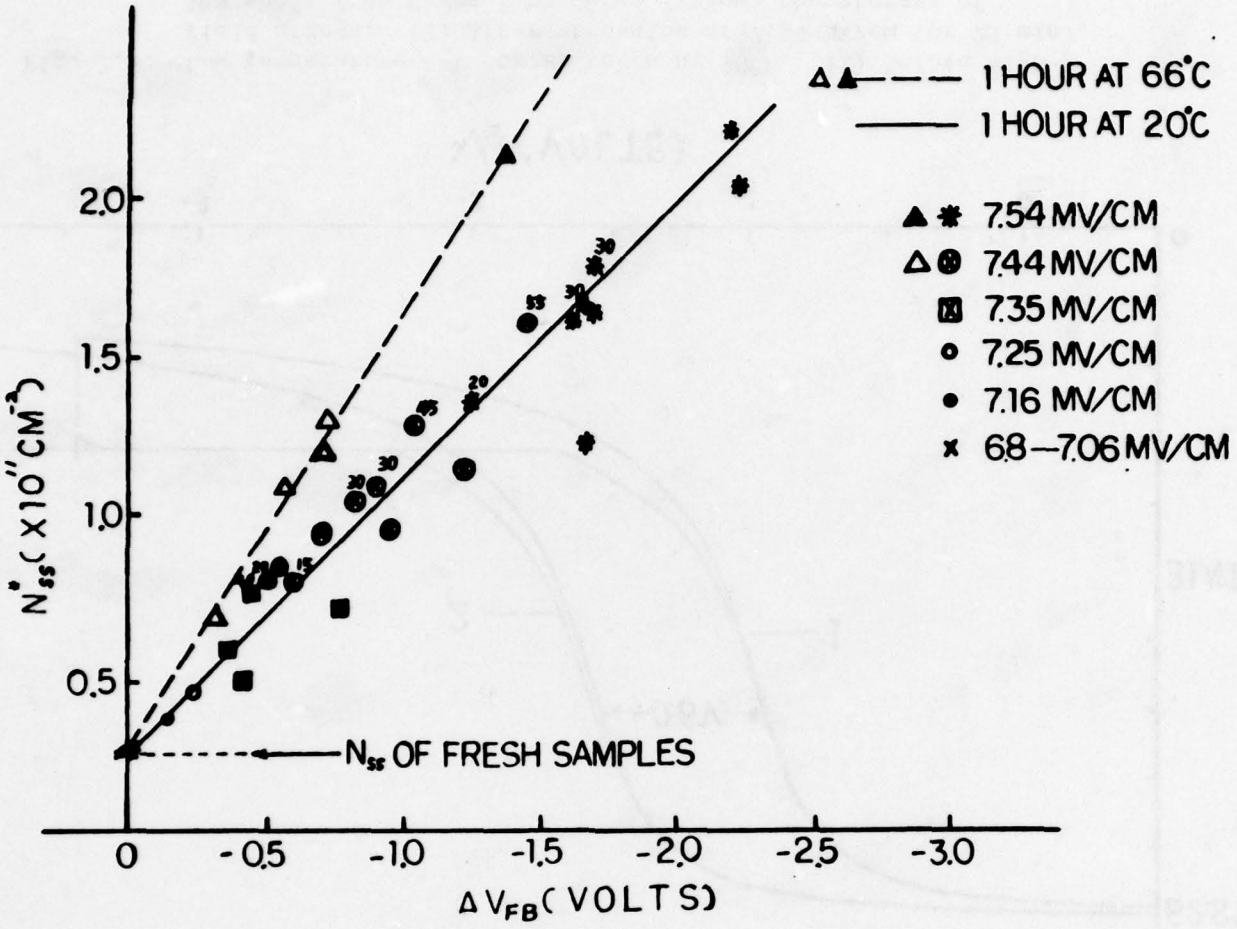

Fig. 2.6. Plot of N^*_{ss} vs ΔV_{FB}, where N^*_{ss} is the value of N_{ss} measured one hour after warmup and ΔV_{FB} is the change of flat-band voltage due to high-field stress. The stress times are 25 min unless otherwise noted beside the plotted point.

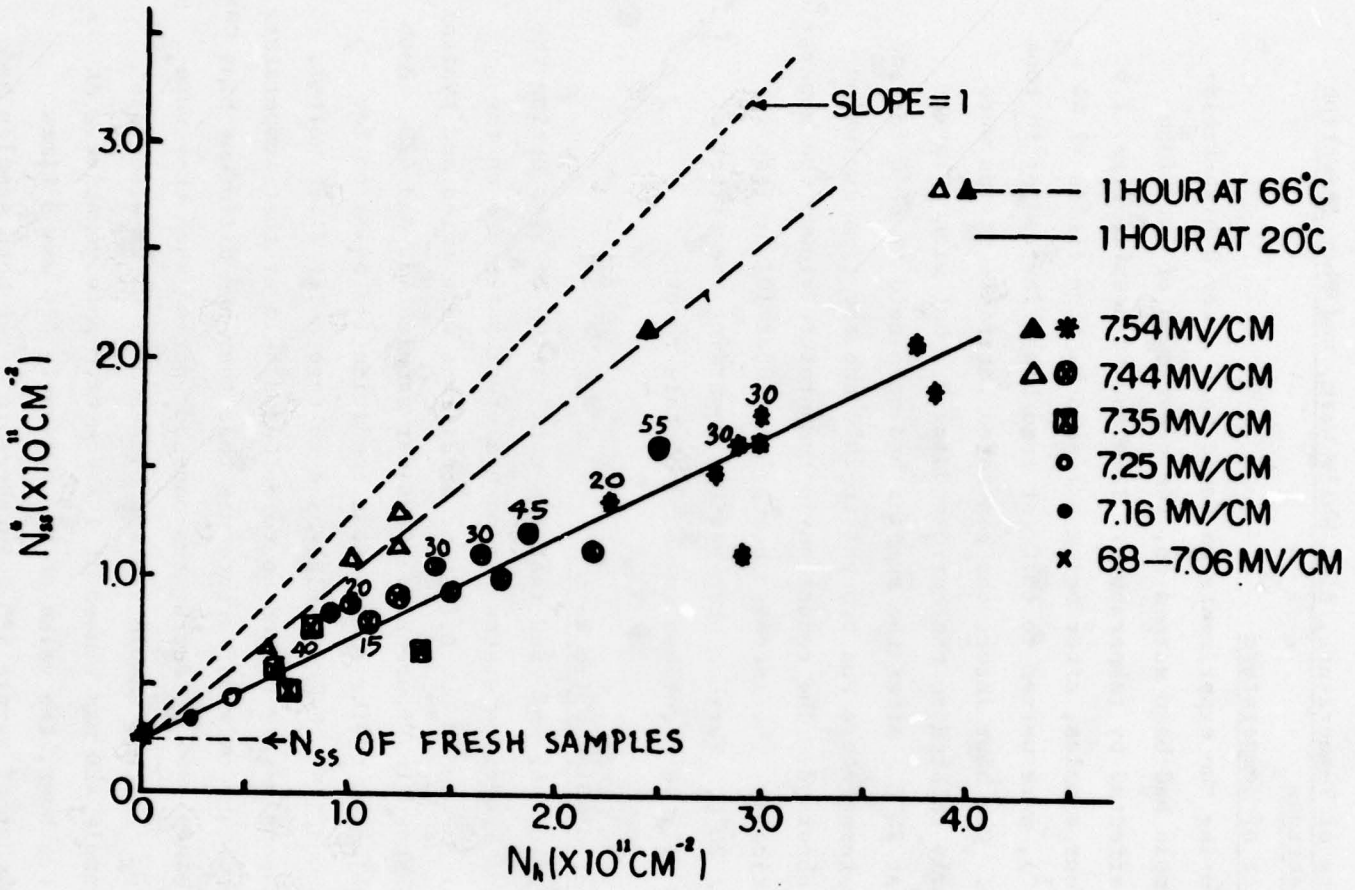

Fig. 2.7. Similar to Fig. 2.6, but with N^*_{ss} plotted against the number of holes trapped at the interface, N_h (cm^{-2}). The line with the slope of unity indicates the relation that would hold if each hole trapped at the interface produced one interface state.

2.5. Effects of Temperature, Bias While Warm, and Photoinjection of Electrons

2.5(A) Effect of Temperature

During the experiments we found that after a high-field-stressed sample had been warmed up, the generation of interface states was affected by temperature. This can be seen in Figs. 2.6 and 2.7. Four samples, after being stressed by high fields (7.44 - 7.54 MV cm^{-1}), were warmed to 66°C (at zero bias) instead of to room temperature. One hour later, the generated interface states were still linearly related to the corresponding N_h, but with a larger slope than at 20°C. After the samples had been held at 66°C for one hour, their temperature was brought to 20°C and the time evolution of N_{ss} was observed. The reduction in temperature slowed the generation rate dramatically, the increase being only about 10% or less in 10^3 hours at 20°C. Further observations regarding the effect of temperature will be described in Ch. 3 of this report.

2.5(B) Effect of Bias While Warm

We further observed that the application of bias during the generation of interface states period had great influence on the formation of N^*_{ss} and N_{ss}. Different conditions were tried and typical results are shown in Figure 2.8. Consider samples 42C and 42D. Both had been subjected to the same stress condition (+7.54 MV/cm for 25 min), showed the same flat-band voltage shift (1.58 volts), and simultaneously were warmed up to 66°C and held at that temperature for one hour. The only difference was that they had different bias conditions while warming and during the one-hour period when they were held at 66°C. Whereas sample 42C was biased at 1 MV/cm with gate positive, sample 42D was biased at 1 MV/cm with gate negative. At the end of the hour, the value of N^*_{ss} of sample 42C was 3 times larger than that of sample 42D. Furthermore after both samples had been brought to room temperature, N_{ss} of sample 42C showed little increase but N_{ss} of sample 42D showed a rather fast increase for about 30 hours. The final difference between the two was still large.

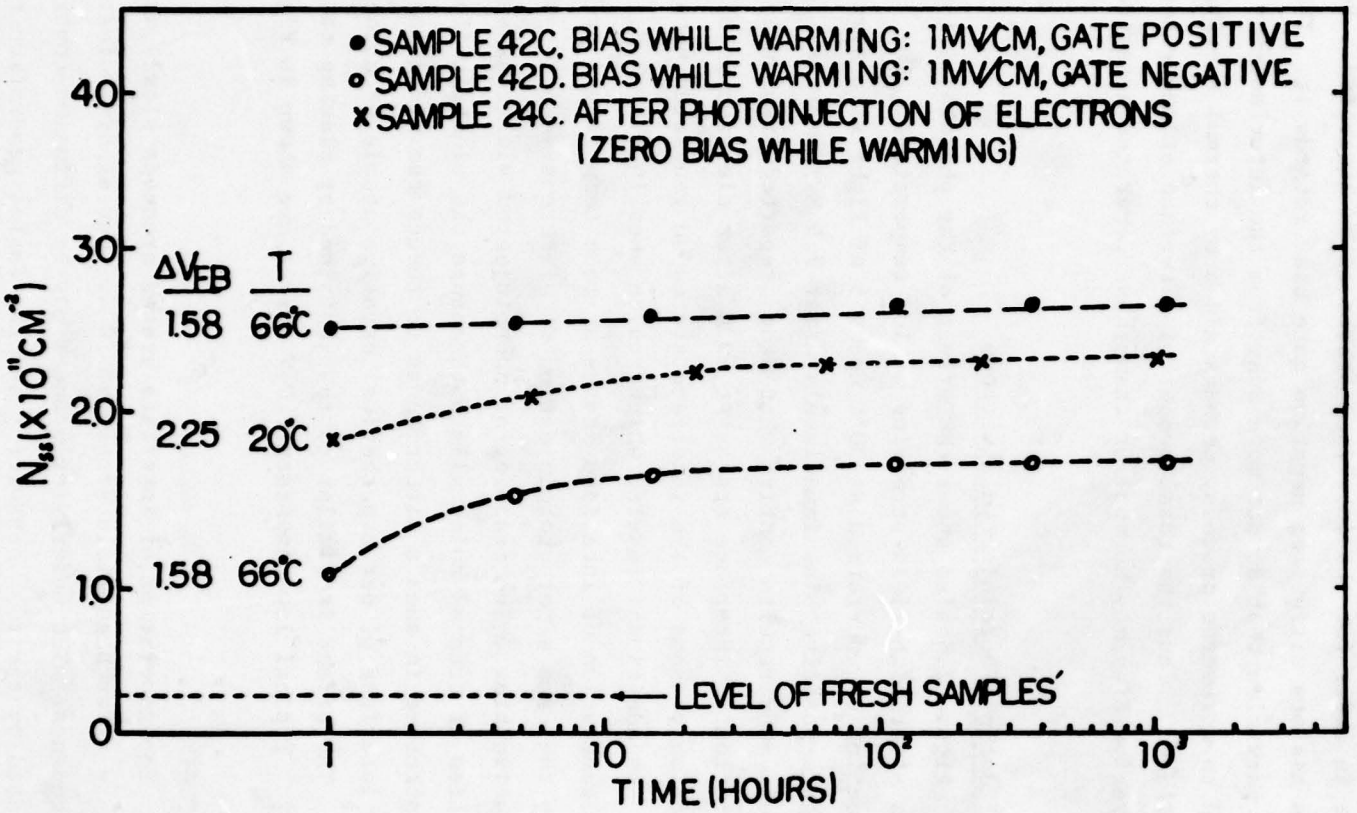

Fig. 2.8. Showing the effect of bias applied while the sample is warmed, and the effect of photoinjecting electrons just before warming. After high-field stress and warming, the sample was held for one hour at either 20°C or 66°C (see column labeled "T") and was then held at room temperature for approximately 10^3 hours.

The strong dependence of N_{ss} on the bias that is applied during interface-state generation suggests the following model. Exposure to the high field releases a negatively charged atomic or molecular species. These charged entities must move away from the interface in order for the interface states to be generated. Positive gate bias assists diffusion; negative gate bias retards it. Those negative particles that do not move away from the interface may be subjected to a reverse process, perhaps aided by thermal energy, and be annihilated. Thus the total number of interface states generated after negative bias may be smaller than those generated after positive bias.

2.5(C) Effect of Photoinjected Electrons

Figure 2.8 also shows the effect of the photoinjection of electrons after high-field stressing at low temperature. The photoinjection was performed at 90°K using 5 eV light with simultaneous 1 MV/cm gate-positive bias immediately after 7.5 MV/cm stress for 25 minutes. Our results confirm what Jenq[4] reported previously: (a) The generation of interface states at 90°K after electron injection. (b) Reduction of some of the interface states so generated upon warming. An additional result, which can be seen in Fig. 2.8, is that the generation of interface states at room temperature proceeds very much the same after photoinjection of electrons as after warming with negative bias. The trapping of photoinjected electrons and the annihilation of trapped holes will both change the electric field at the interface in such a direction as to reduce the migration away from the interface of our hypothetical negative atomic or molecular species. The effect is similar to that obtained by biasing the gate negative. Typical low-temperature C-V curves are shown in Fig. 2.9.

2.6. Summary

The generation of interface states proceeds slowly at room temperature after high-field stress at 90°K. Our study indicates a $t^{1/4}$ dependence. The underlying process may be diffusion-controlled, as indicated by the $t^{1/4}$ behavior[11] and the faster generation rate observed at higher temperatures. The effect of bias polarity while

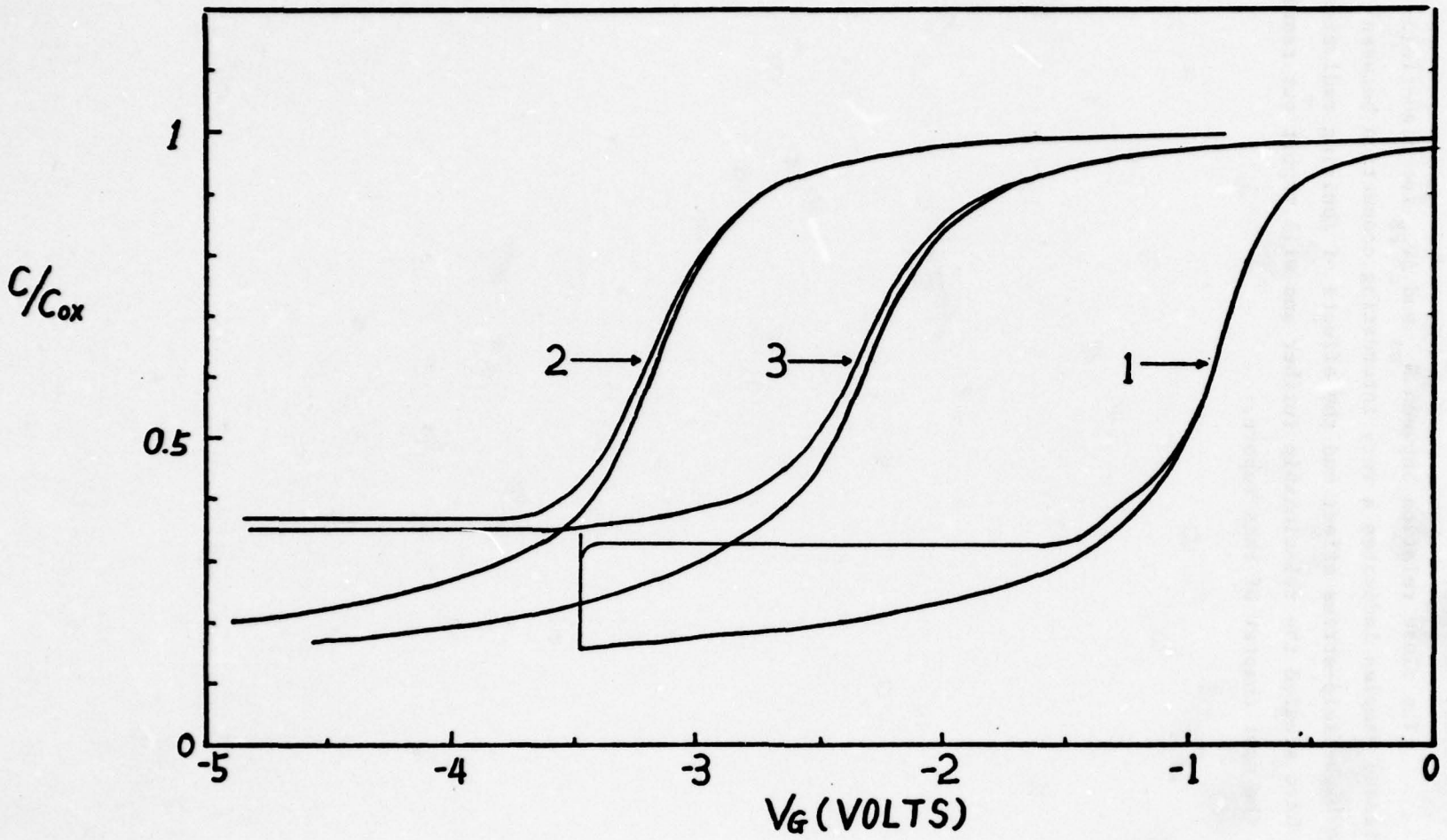

Fig. 2.9. The effect of high-field stress followed by photoinjection of electrons at 90°K. (1) Fresh condition. (2) After stress at high field (7.54 MV/cm for 25 min). (3) After injection of electrons through $Si-SiO_2$ interface using 5 eV light. $Q_{injection} = 2.2 \times 10^{-6}$ coulombs/cm^2.

the generation is taking place may indicate that the diffusing species is negatively charged.

The close relation between N_{ss} and ΔV_{FB} for high-field stressed samples indicates a very interesting connection between the high-field-stress effect and the effects of ionizing radiation. We have studied the relationship further and will report our results in the next chapter of this report.

3. COMPARISON BETWEEN THE EFFECTS OF HIGH FIELD STRESS AND IONIZING RADIATION IN GENERATING INTERFACE STATES IN MOS CAPACITORS

(Genda Hu collaborating)

3.1. Introduction

In the preceding chapter we mentioned the conjecture that radiation-hard MOS structures (which trap few holes) should show a correspondingly smaller generation of interface states after exposure to high electric fields. We base this on the hypothesis that holes, no matter how created, can, when located near the $Si-SiO_2$ interface, cause the generation of interface states. The generation process requires the aid of thermal energy. We have performed a number of experiments in order to test this assumption. A comparison of the similarities and differences between high-field effects and radiation effects with regard to the generation of interface states may aid in our understanding of the origin and physical nature of the interface states.

3.2. Samples and Experimental Procedures

All the samples used here were similar to those described in the preceding chapter. They had n-type silicon substrates and dry-grown oxides of 1190Å thickness.

Unless otherwise specified, the general experimental procedures were as follows: After recording the initial high-frequency and quasistatic C-V curves at 66°C, the MOS capacitor sample was cooled to liquid nitrogen temperature, and the initial interface-state density was measured by the LTD method.[6,7] The sample was then exposed to soft x-rays in the manner previously described by J. J. Clement.[6] The typical irradiation time was 3 minutes, and the electric field applied to the sample was field-plate-positive 1 MV/cm. However, in order to get different irradiation conditions for comparison, we sometimes varied the magnitude and polarity of the bias field during the irradiation and sometimes altered the x-ray exposure time. Soft x-rays will generate electron-hole pairs in the oxide;[20] the electrons are rapidly swept out by the bias field, the holes are left behind and will cause a negative shift of the flat band voltage. This flat-band voltage shift (ΔV_{FB}) can be varied by changing the bias field or the exposure time.

After recording the magnitude of the shift, we warmed the sample either to room temperature or to 66°C. In some cases, internal photoinjection of electrons was performed at liquid nitrogen temperature with 5 eV light while simultaneously applying 1 MV/cm gate-positive bias. Generally, this was done after the soft x-ray irradiation and before the first warmup.

All the data were deduced from C-V curves. Low temperature curves were taken at liquid nitrogen temperature. High-frequency and quasistatic C-V curves were taken at 66°C rather than at room temperature so that thermal equilibrium could be maintained with reasonable sweep rates.

In addition to the irradiation experiments, corresponding high-field-stress experiments were also carried out, following the procedures that were described in the previous chapter.

3.3. Results

3.3(A). Holes and Interface States

In order to see how trapped holes, when produced by x-irradiation, are related to the generation of interface states, we have plotted N_{ss}^{*} vs. ΔV_{FB} in Fig. 3.1, where N_{ss}^{*} is the density (cm^{-2}) of interface states measured one hour after the irradiated sample had been brought either to room temperature or to 66°C, and ΔV_{FB} is the flat-band voltage shift caused by x-irradiation at low temperature. Comparing this plot with Fig. 2.6, we are struck by the amazing resemblance between the two. Again we have the linear relation between N_{ss}^{*} and ΔV_{FB} which indicates that radiation-induced interface states also correlate with excess holes in the oxide. We find, however, that there also exists a difference between the two. The slopes of the lines in Fig. 3.1 are 10-15% smaller than those in Fig. 2.6. This difference may be explained by either of the following reasons: (a) Experimental error. During the soft x-ray exposure process, the shadow of the probe on the field plate introduced a lateral nonuniformity in the irradiation. This lateral nonuniformity led to some difficulties in determining the values of ΔV_{FB}. This uncertainty in ΔV_{FB}, although small, may be the reason for the differences in slopes between the two figures.

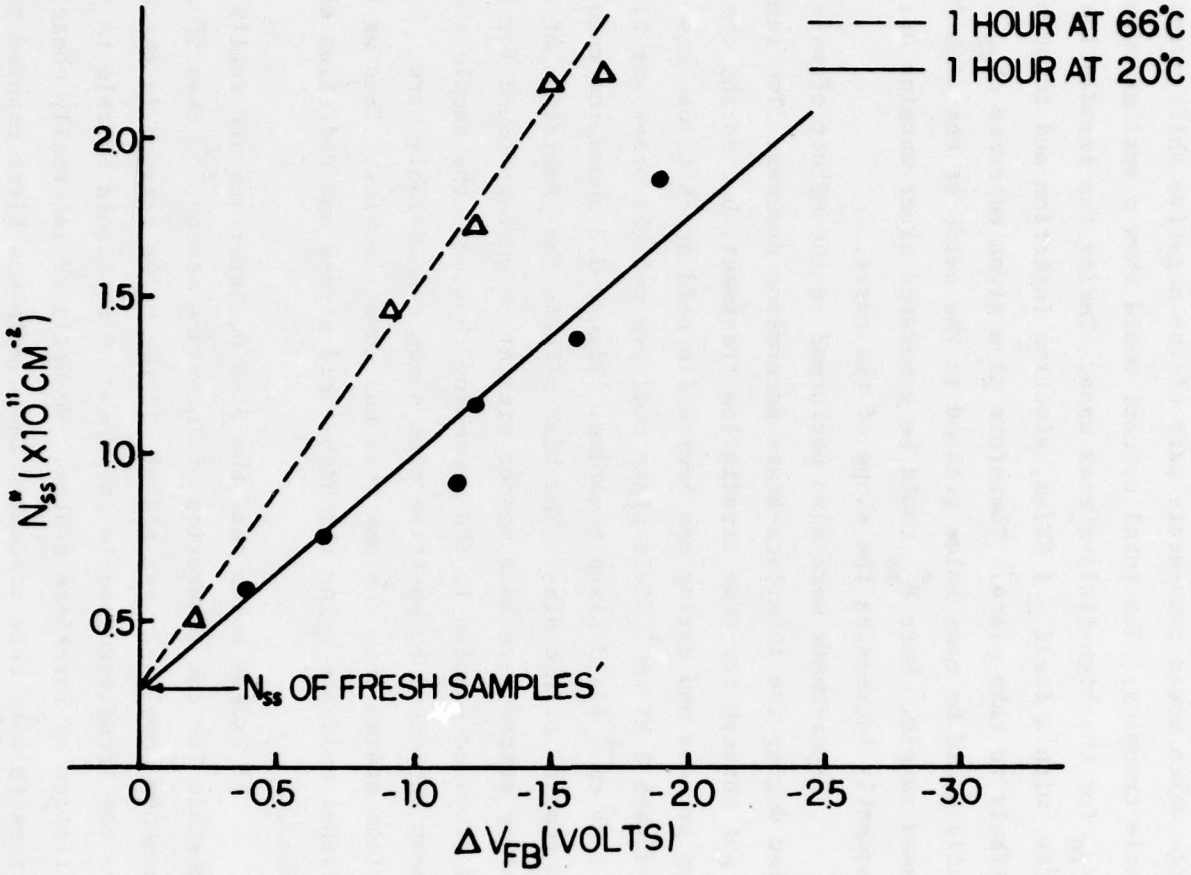

Fig. 3.1. Plot of N^*_{ss}, the generated interface state density one hour after warmup, vs. ΔV_{FB}, the shift of flat-band voltage caused by the irradiation by soft x-rays.

(b) Some electron traps in the bulk of the oxide may have been filled when the large quantity of electrons flowed through the oxide; for instance, during the high-electric-field stress process.[14] These trapped electrons would cause a positive shift in the flat band voltage which would compensate part of the negative shift owing to the hole trapping. The total outcome would show a smaller value of ΔV_{FB} for the high-field-stress case. During the irradiation process, with a field $\leq$ 1 MV/cm, electron injection and trapping is not likely to take place. Therefore at a given measured ΔV_{FB}, there actually could be more holes trapped in the oxide of the high-field-stressed sample. More N_{ss}^{*} could be generated after warming up, consequently increasing the slope of the curve.

Experiments were also performed on the effect of bias applied during the interface-state generation process. Two samples were put through the same irradiation treatment, but during the warmup process and during one hour while held at 66°C, one was biased with 1 MV cm^{-1} field-plate positive and the other was biased with 1 MV cm^{-1} field-plate negative. Figure 3.2 shows the results after removal of the bias. The bias affects the generation of interface states here in a manner similar to what we found for high-field stressed samples in the preceding chapter: the sample that had been subjected to positive bias shows considerably more interface states than the one that had negative bias. Thus we find additional evidence tying the high-field stress and radiation effects together.

If excess holes near the Si-SiO_2 interface are really responsible for the generation of interface states,[2,4] then if we can somehow completely get rid of all the holes trapped in the oxide before the irradiated sample is warmed up we should be able to prevent any creation of interface states. We utilized internally photoinjected electrons to test this concept. The sample was first exposed to soft x-rays for 3 minutes with a field-plate-positive bias of 12 volts ($\approx$ 1 MV/cm), then, with the same bias condition, 5 eV light was used to photoinject electrons from the silicon substrate into the oxide. After more than three hours, approximately 1.0×10^{14} electrons per cm^2 had been injected. Figure 3.3 shows the time evolution of the low-

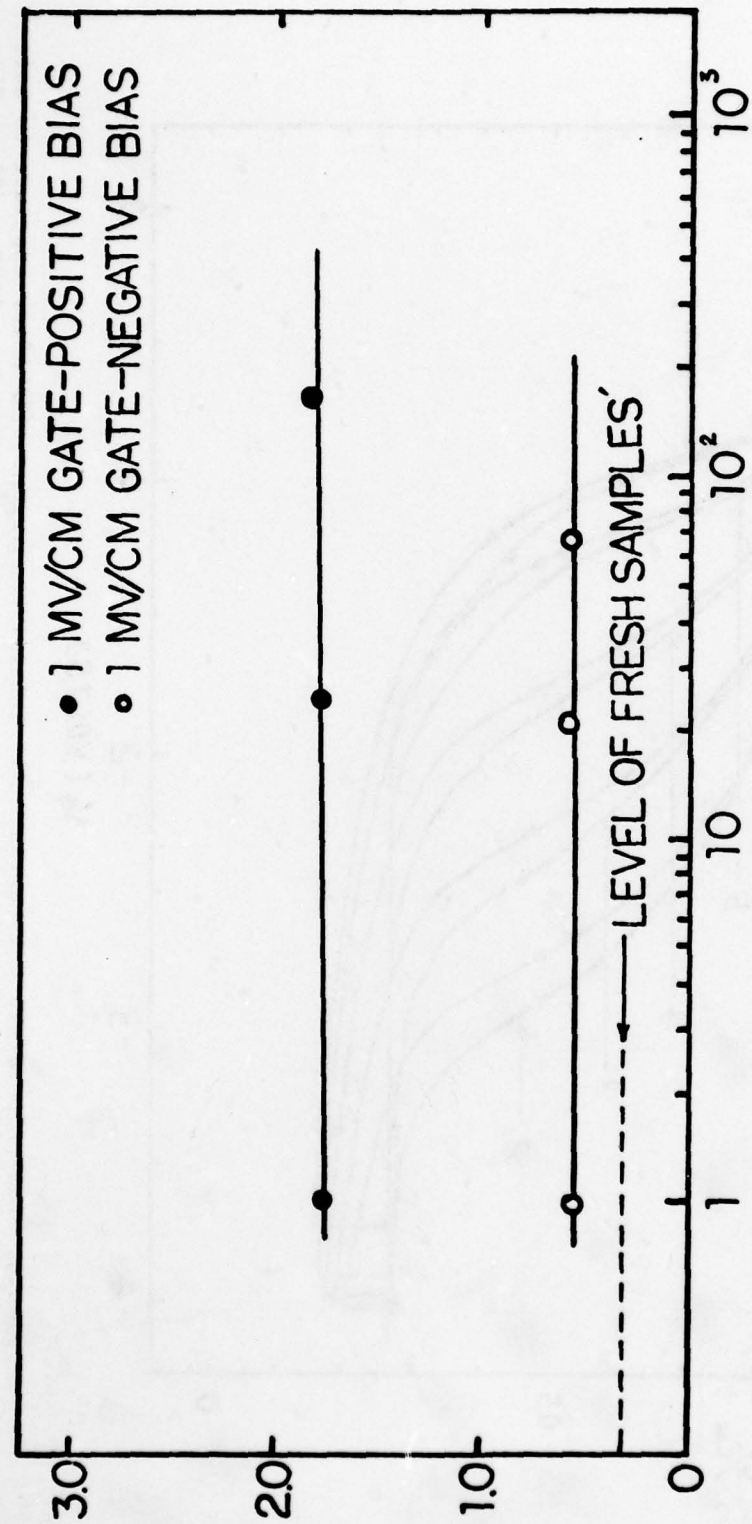

Fig. 3.2. Plot of interface-state density vs. time at room temperature. The samples had been cooled to 90°K and exposed to soft x-rays for 3 min with 1 MV/cm gate-positive bias. This was followed by warming to 66°C (∿ 20 min) and holding at 66°C for one hour, during all of which time a positive or negative bias of 1 MV/cm was applied. The data points shown above were taken after cooling to room temperature (field plates floating).

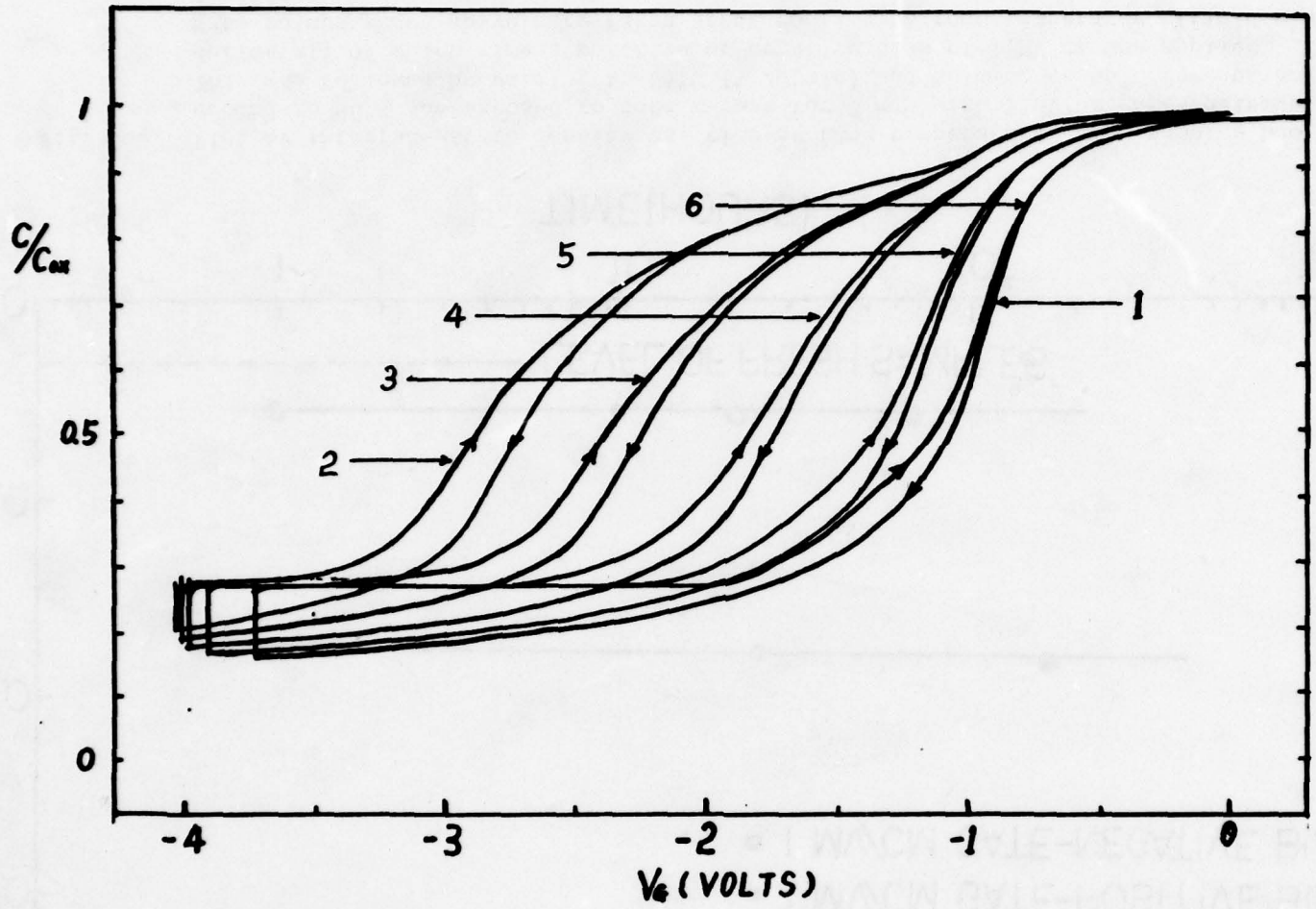

Fig. 3.3. Low-temperature C-V curves. (1) Initial condition. (2) After exposure to soft x-rays for 3 min with 12 V gate-positive bias ($\approx$ 1 MV/cm) at 90°K. (3) to (6): The time evolution of the C-V curves after photoinjecting 1.0×10^{13}, 2.4×10^{13}, 7×10^{13}, and 1.0×10^{14} electrons/cm^2 respectively, from Si into the oxide. Note that (6) is identical with (1). The distortion in Curves 2-4 is caused by the shadow of the probe during x-irradiation.

temperature C-V curves during this experiment. We can see that the final set of curves (6) is shifted back to its original position and shape by the electron injection; thus all holes were presumably recombined with electrons. The sample was then warmed to room temperature. Even after several days, both the LTD method[6,7] and Kuhn's method[15] were used to measure the density of interface states, and we did not find any increase in this sample in which the holes had been annihilated before warmup.

We now turn our attention to the effect of high-field stress. We reported a similar photoinjection experiment in Ch. 2, but in that experiment we did not annihilate all the holes as we shall do here. The C-V curves of Fig. 3.4, which were taken at 90°K, show the results of this experiment. Curves 1 are the initial deep depletion and light-assisted curves required for the LTD method.[6,7] Curve 2 was obtained after stress at 7.54 MV/cm for 15 minutes at 90°K. The leftward shift shows the presence of high-field-created holes. Curve 3 was taken after we attempted to annihilate all the holes by photoinjecting electrons (1×10^{14} cm^{-2}). Curve 3 is seen to have overshot to the right of the original curve by about 0.3V, and the shape was not exactly preserved. This is different from the results of the irradiation experiment (Fig. 3.3), and we believe it to be the consequence of electron trapping in the oxide.[4-8] The trapping may take place either during the high field stressing or during the photoinjection. Moreover, after the sample was warmed we find from Curves 4 of Fig. 3.4 that there was some generation of interface states. The amount of these is not great, about 0.7×10^{11} cm^{-2}, but it is a result somewhat different from that obtained after x-irradiation. Possible explanations are: (a) These interface states are different in character from the type we ordinarily observe, for it was further observed that they hardly increase at all when the sample is held for a long time at room temperature. They may be associated with a high-field effect such as the generation of electron traps,[4-8] an effect which we have not observed in our samples irradiated with soft x-rays. (b) Because of the shielding effect imposed by the trapped electrons near the $Si-SiO_2$ interface, we may not be able to recombine all the holes by photoinjecting electrons. The leftover holes could cause the generation of interface states. Since the interface states that we observe are so few

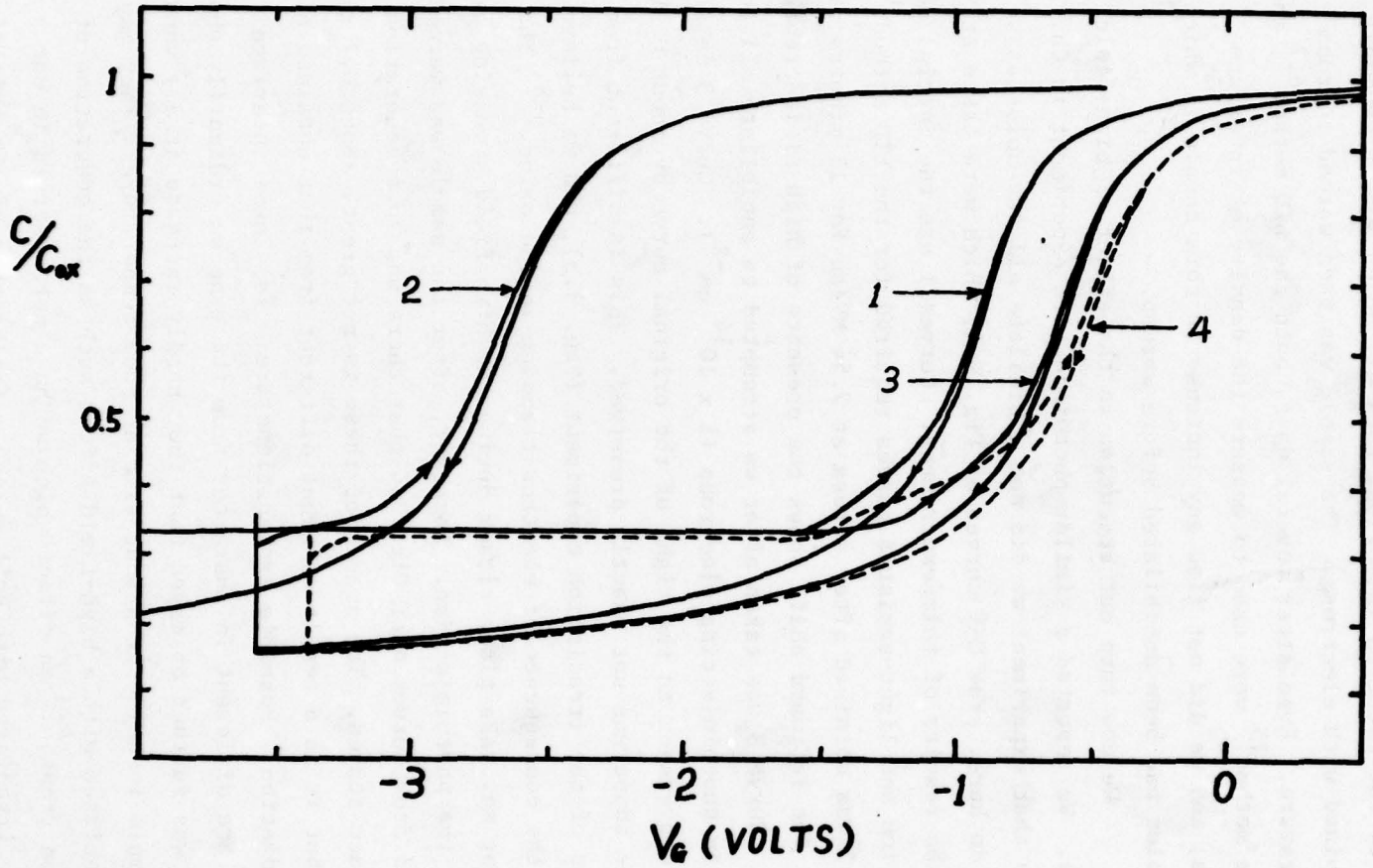

Fig. 3.4. Low temperature (90°K) C-V curves. (1) Initial condition. (2) After high-field stress at 7.54 MV/cm for 15 min. at 90°K. (3) After photoinjecting 1.0×10^{14} electrons cm^{-2} from Si into oxide. (4) After the sample had been warmed to room temperature and held for 1 hour.

in number, the process of continued generation at room temperature is not prominent.

3.3(B). Energy Distribution of Interface States in the Silicon Bandgap

Determination of the energy distribution of the two types of interface states (high-field-stress induced and radiation induced) in the silicon bandgap is important for our comparison studies. If the generation of these two types of interface states share the same mechanism, the interface-state densities should have identical energy distributions.

The energy distribution curves were calculated using the quasistatic C-V curve technique as described by Castagne[16] and Kuhn.[15] This method is useful within a region limited to about $\pm$ 0.3 eV[17] around midgap. All of the quasistatic C-V curves were taken at 66°C to allow thermal equilibrium to be maintained at reasonable sweep rates. Because lateral nonuniformities in the sample can cause serious error in calculating the distribution function, a shadow of the probe on the surface of the field plate must be avoided. To accomplish this we moved the probe away and let the gate float without bias field during the irradiation. Electron-hole pairs therefore recombined more easily after generation by high-energy photons.[18,19] In order to get enough holes trapped in the oxide, we extended the x-ray exposure time (previously 3 min) to 30 min.

One sample was subjected to high-field stress (7.5 MV/cm for 15 min at 90°K), and the other was irradiated with soft x-rays (30 min at 90°K with gate floating). The samples were warmed (in 15 min) to 20°C and held at 20°C for one hour. The samples were subsequently held for one hour each at 66°C, 95°C, 120°C, and 150°C (also 180°C for the high-field-stressed sample). At the end of each hour the temperature of the sample was brought briefly to 66°C for measurement of the quasistatic C-V curves. The results of these measurements are shown in Fig. 3.5 for the high-field stressed sample and in Fig. 3.7 for the x-irradiated sample. The two sets of curves are seen to be quite similar. The energy distribution of the interface states was calculated from the quasistatic curves by the Kuhn-Castagne method,[15,16] with the results shown in Figs. 3.6

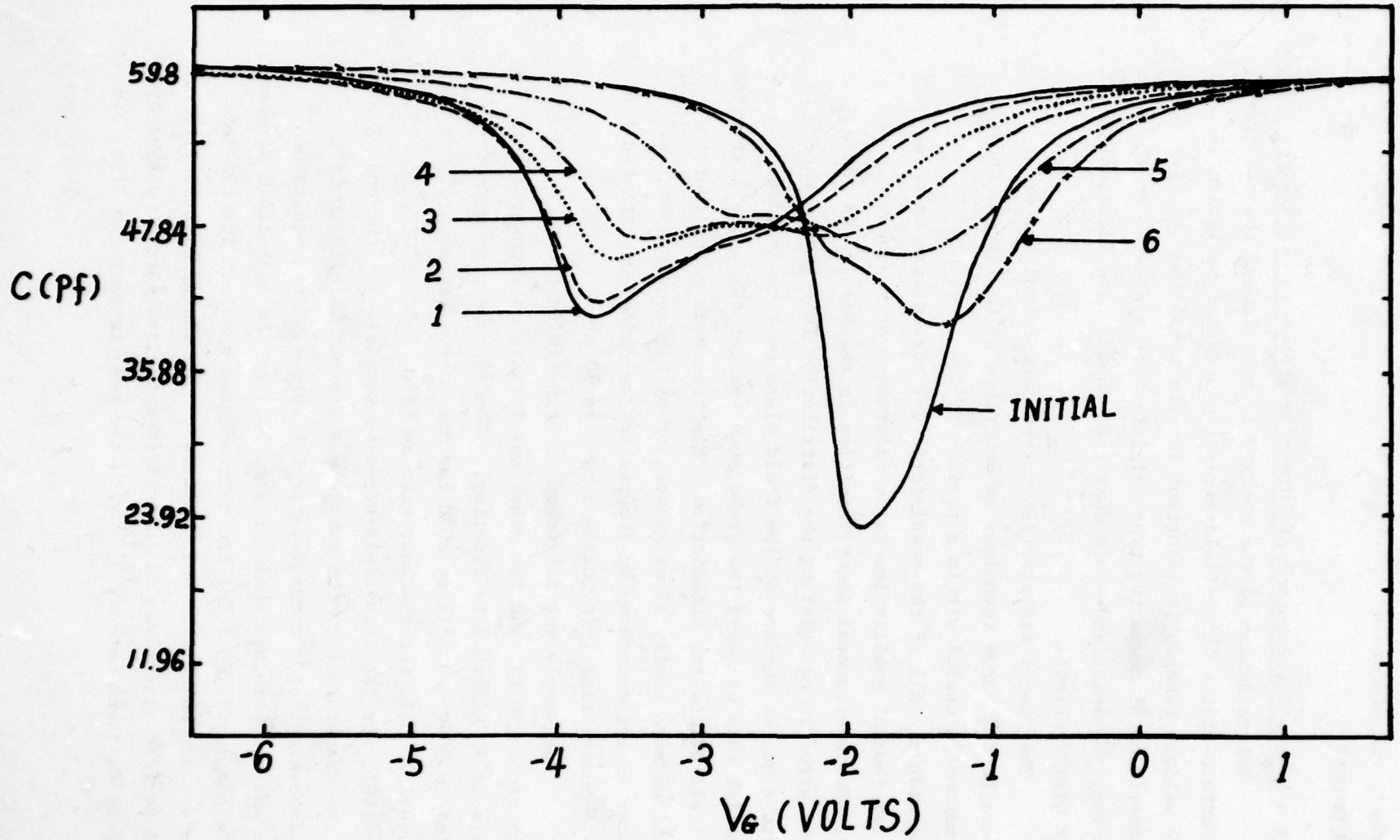

Fig. 3.5. Showing the effect of high field stress (7.5 MV/cm for 15 min at 90°K) on the quasistatic C-V curves (taken at 66°C). The initial curve is included for comparison. After stressing at 90°K, the sample was warmed (in 15 min) to 20°C and held there for one hour, resulting in Curve 1. Heating, and holding the sample successively at 66°C, 96°C, 120°C, 150°C, and 180°C, resulted in Curves 2-6, respectively.

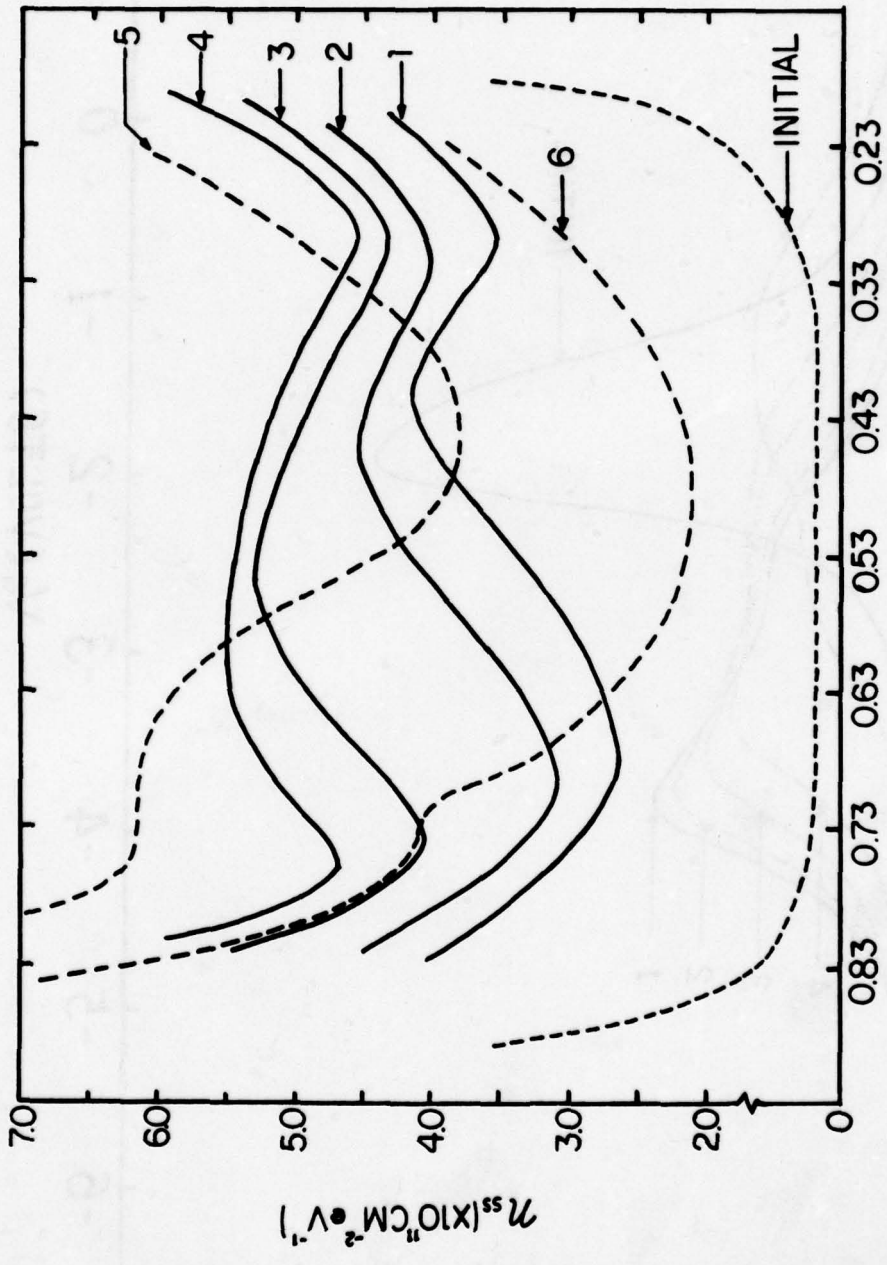

Fig. 3.6. Energy distribution of interface states in the Si bandgap after high-field stress and warming. All the curves were calculated from the corresponding quasistatic C-V curves shown in Fig. 3.5.

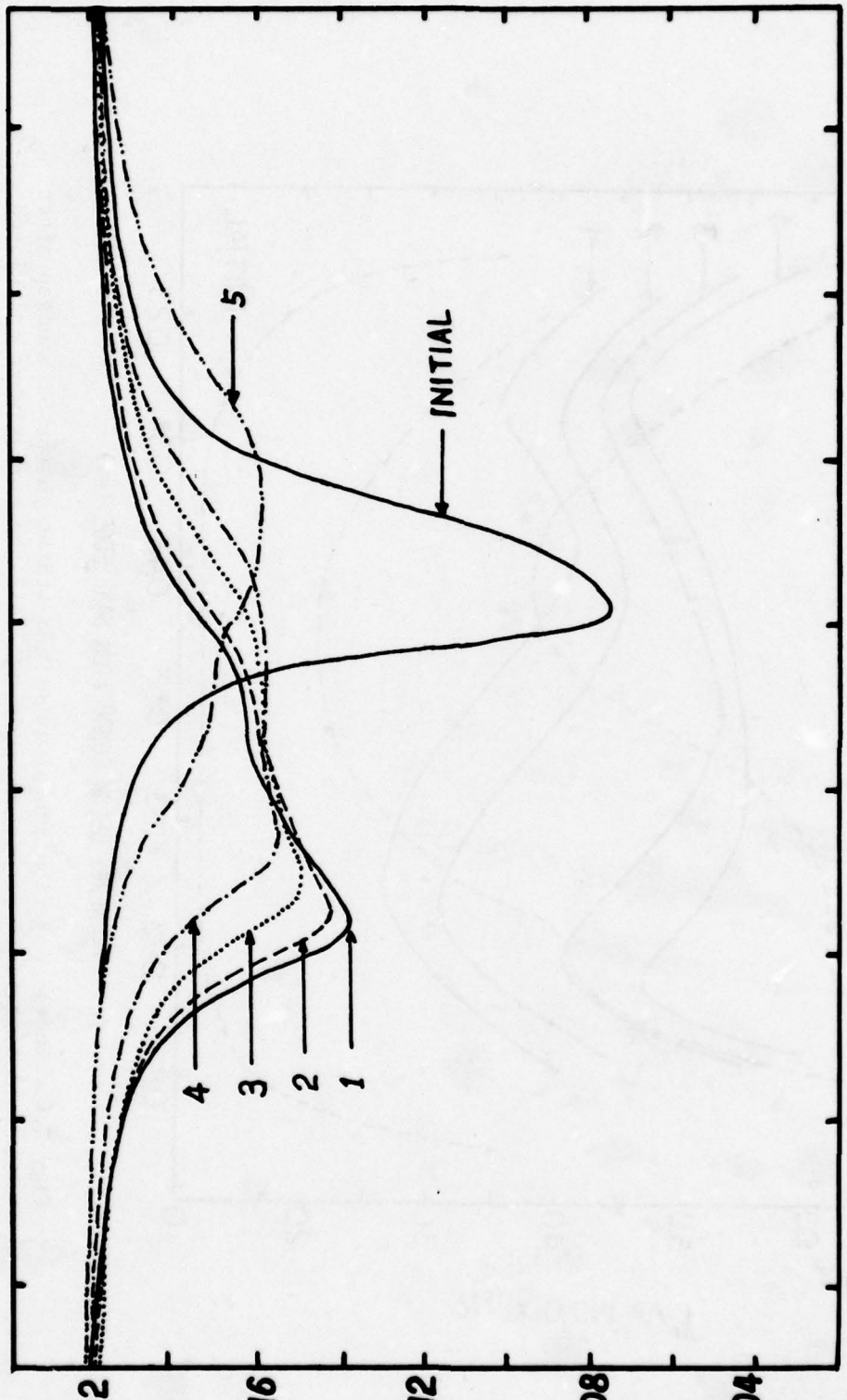

Fig. 3.7. Quasistatic C-V curves similar to those of Fig. 3.5 but showing the effect of exposure to soft x-rays for 30 min at 90°K with gate floating. The sample was subsequently held for one hour each at 20°C, 66°C, 96°C, 120°C, and 150°C. This yielded Curves 1-5, respectively.

and 3.8. Again, these two figures show considerable similarity. An unexpected property is that the energy distribution function does not have a peak located at a fixed energy, but instead the peak moves in energy with both temperature and time. From Figs. 3.6 and 3.8 we can see that (a) The peak of the distribution moves away from the conduction band edge as temperature goes up. (b) The interface states start to anneal out when the temperature is high. (The detrapping of holes, as determined from ΔV_{FB}, turns out to become prominent at the higher temperatures.) (c) The behavior of the peak located at about 0.43 eV is somewhat different in Fig. 3.8 than in Fig. 3.6. We shall discuss these points later in this chapter.

Figure 3.9 shows the evolution of n_{ss} after a fresh sample was stressed by an electric field of 7.44 MV cm^{-1} for 25 min at 90°K. The sample was then warmed and kept at room temperature except 3 short periods when we took the quasistatic C-V curves at 66°C. Curve 1 was taken 1 hour after the stress, Curve 2 was taken after 21 hrs, and Curve 3 was taken 6 months later. Here we can see the peak shift from 0.43 eV to about 0.50 eV below the conduction band.

In order to perform an experiment in which the 66°C temperature perturbation was kept to a minimum, we stressed 5 more samples with fields between 7.44 and 7.54 MV/cm for 25 min at 90°K and then let them sit at room temperature (occasionally we took measurements by the LTD method at 90°K). Seven months later, for the first time, we quickly warmed the samples to 66°C and took the quasistatic C-V curves. The results are shown in Fig. 3.10. All the n_{ss} peaks lay about 0.53 eV below the conduction band edge. If we use Curve 1 of either Fig. 3.6 or Fig. 3.9 as an initial curve, again we see the shift of the n_{ss} peak under the influence of time, not of temperature.

Another sample was stressed by an electric field of 7.54 MV cm^{-1} at 90°K, then it was directly warmed to 66°C and held at that temperature for 6 hours. Figure 3.11 shows the results. Curve 1 was taken immediately after the sample was warmed to 66°C. Curve 2

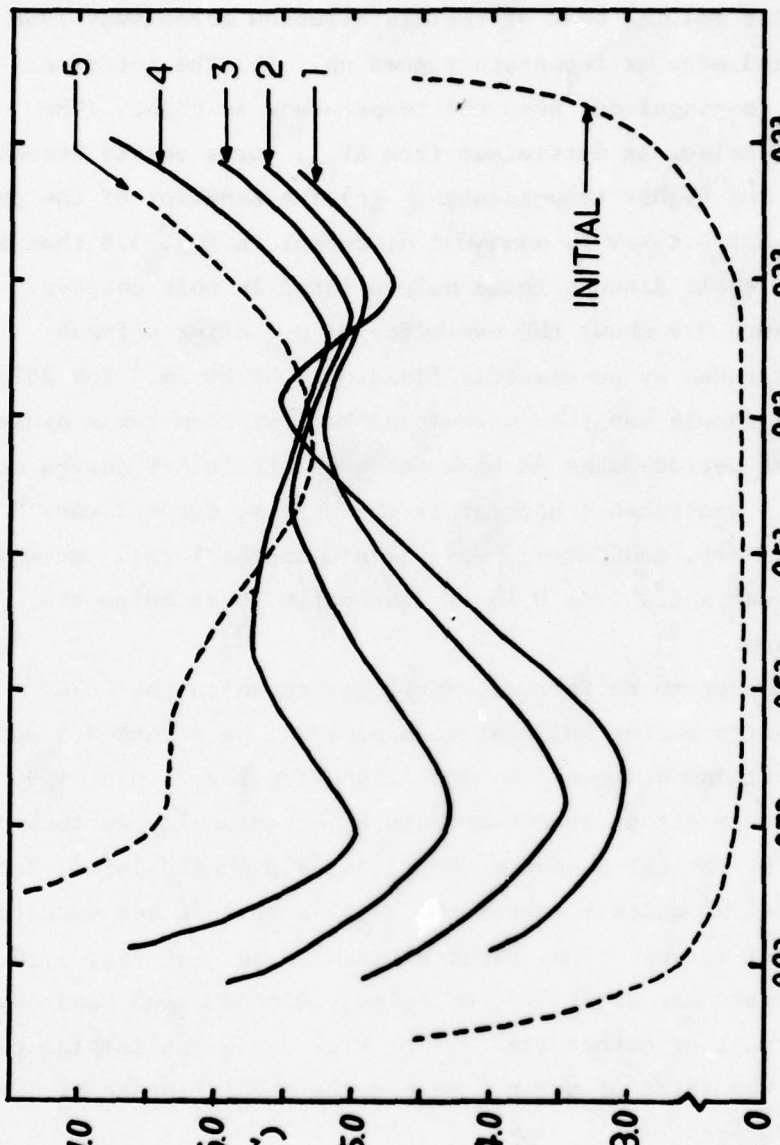

Fig. 3.8. Energy distribution of interface states in the Si bandgap after x-irradiation and warming. All the curves were calculated from the corresponding quasistatic C-V curves shown in Fig. 3.7. These results can be compared with those of Fig. 3.6, which were obtained after high-field stress.

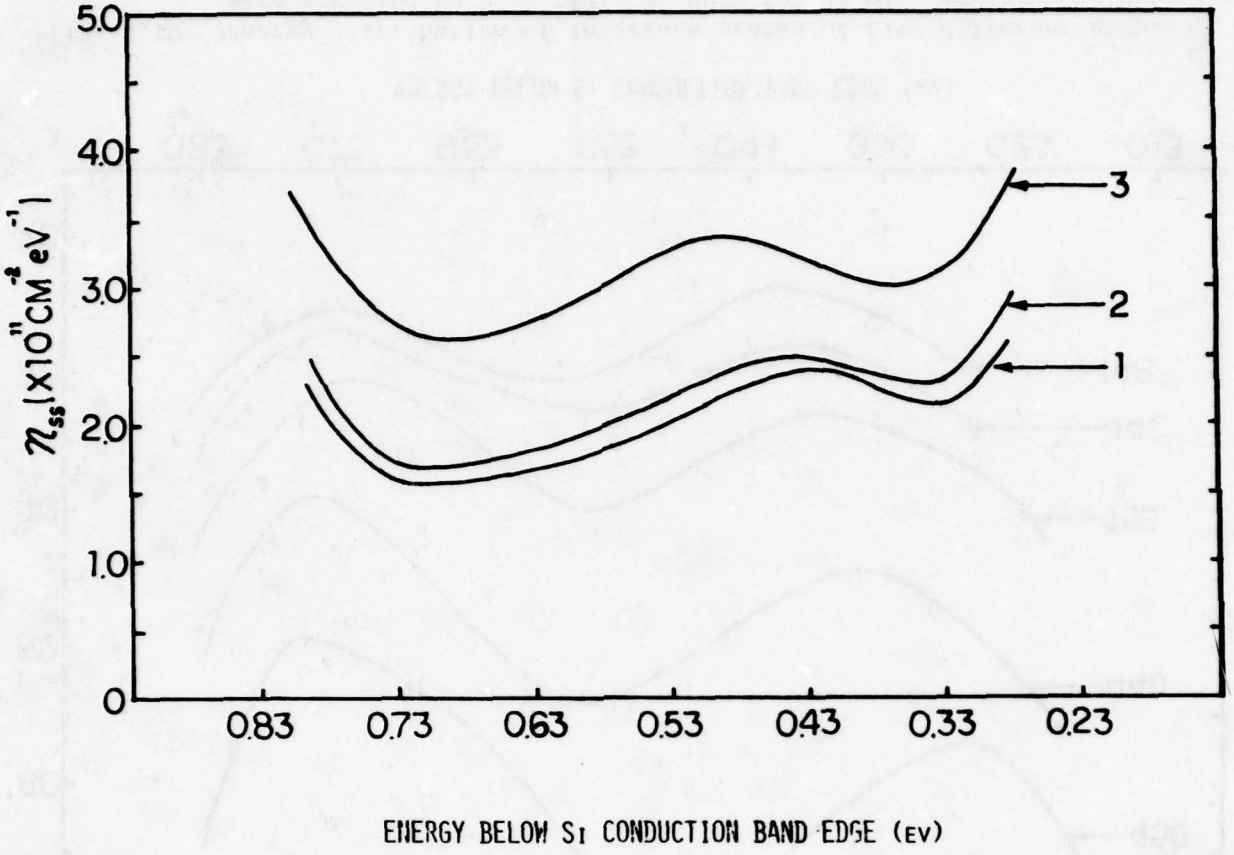

Fig. 3.9. Energy distribution of interface states for a sample stressed by electric field of 7.44 MV cm^{-1} for 25 min at 90°K. Curve 1: After 1 hr at room temperature. Curve 2: After 21 hrs. at room temperature. Curve 3: Six months later.

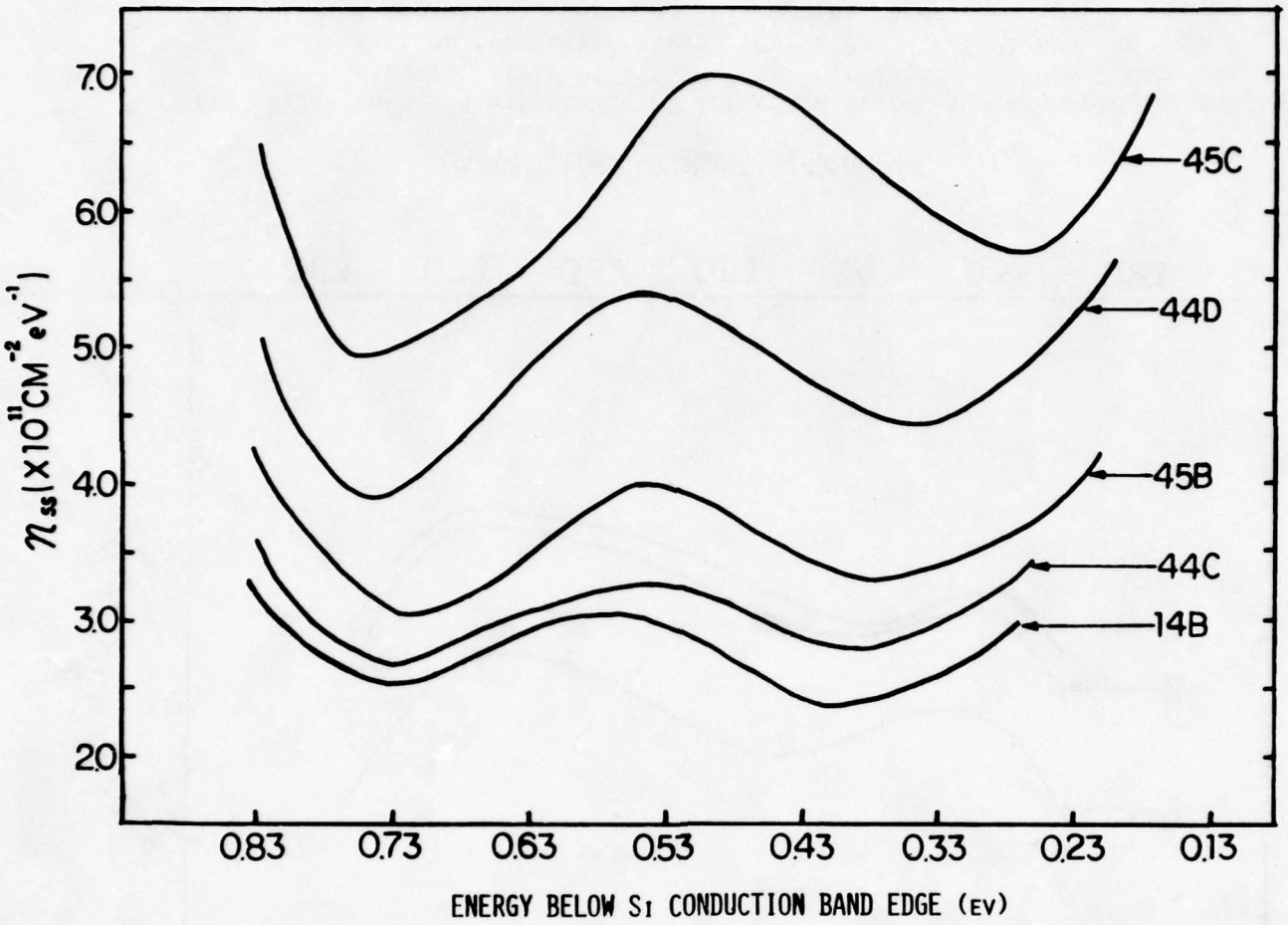

Fig. 3.10. Energy distribution of interface states of five different samples. All were stressed by high field at 90°K for 25 min. and then held at room temperature for 7 months. The stress fields were: sample 14B: 7.32 MV cm^{-1}; samples 44C and 45B: 7.44 MV cm^{-1}; samples 44D and 45C, 7.54 MV cm^{-1}.

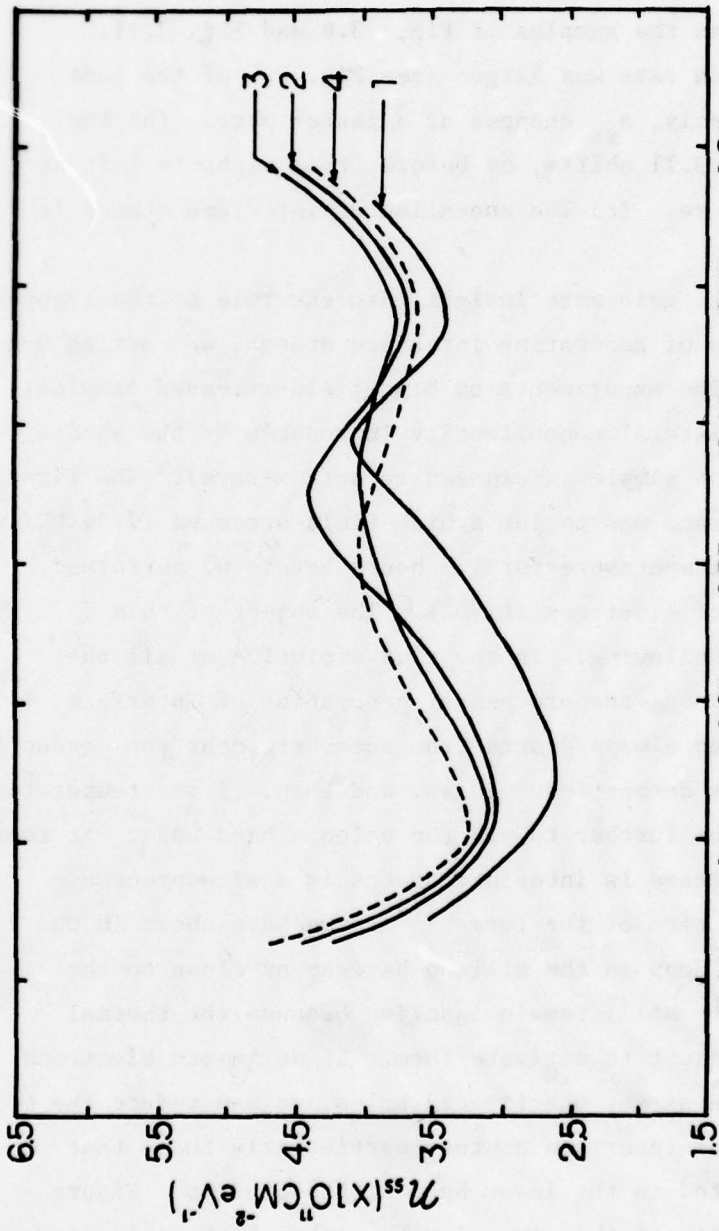

Fig. 3.11. Energy distribution of interface states of a sample that was high-field stressed at 90°K for 15 min with 7.54 MV cm^{-1} and then warmed to 66°C. Curve 1: After 5 min at 66°C. Curve 2: After 1 hr at 66°C. Curve 3: After 2 hrs at 66°C. Curve 4: After 4 hrs at 66°C.

was taken an hour later, and Curve 3 was taken two hours later. After 3 hours the C-V curve changed very little, and the result after 4 hrs. is shown by Curve 4. From these curves we can see: (a) The reduction in peak height is not a unique characteristic of the irradiated samples (shown in Fig. 3.8). Curves 1 and 2 in Fig. 3.6 are certainly equivalent to Curves 1 and 2 in Fig. 3.11, but Curves 1 and 2 in Fig. 3.8 are equivalent to Curves 2 and 3 in Fig. 3.11. This may be due to the sample of Fig. 3.8 having a larger number of interface states than the samples of Fig. 3.6 and Fig. 3.11, and so the generation rate was larger (see Fig. 2.1 of the last chapter). Consequently, n_{ss} changes at a faster pace. (b) The peak of n_{ss} in Fig. 3.11 shifts, as before, from right to left at this fixed temperature. (c) The annealing of interface states is seen even at 66°C.

In order to gain more insight into the role of the trapped holes in the process of generating interface states, we carried out internal photoemission experiments on high-field-stressed samples (thus avoiding the lateral nonuniformity introduced by the shadow of the probe when the sample is exposed to soft x-rays). The first experiment we performed was to let a high-field-stressed (7.54 MV/cm) sample sit at room temperature for 1.5 hours before we performed the photoinjection of electrons at 90°K. The object of this experiment was the following: In the time evolution of all the preceding n_{ss} functions, the process of generation of interface states in the bandgap always starts from somewhere near the conduction band edge, then goes deeper into midgap, and then, if the temperature is high enought, goes further toward the valence band edge. At room temperature the increase in interface states is a slow process, being a function of time of the form $t^{1/4}$ as we have shown in Ch. 2. Those holes trapped deep in the silicon bandgap or close to the valence band edge may still remain inactive because the thermal energy is not sufficient to activate them. If we inject electrons and annihilate those as-yet unactivated holes, we may reduce the further generation of interface states, particularly those that remain to be generated in the lower half of the bandgap. Figure 3.12 shows the results of this experiment. After high-field stressing

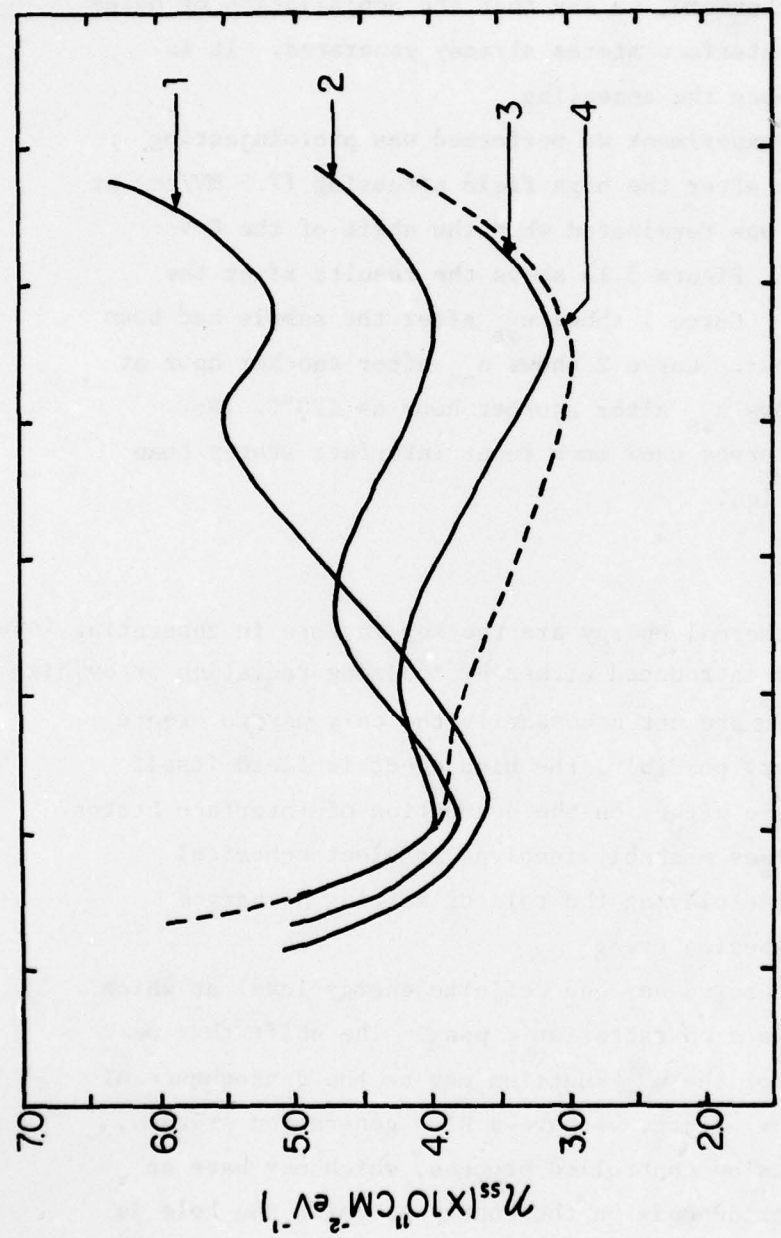

Fig. 3.12. Energy distribution of interface states of a sample that had been stressed at 90°K for 15 min with 7.54 MV/cm, followed by the following steps: First warming to 20°C, then a photoinjection of electron at 90°K, and finally warming to 66°C and higher. Curves 1 through 4 were obtained after the sample had been held one hour each at 66°C, 96°C, 120°C and 150°C.

at 90°K the sample was warmed to 20°C, then it was cooled to 90°K and electrons were photoinjected. Curves 1 through 4 shows the distribution of interface states after warming and subsequent one-hour's stay at 66°C, 96°C, 120°C and 150°C successively. As we predicted, there is only a minor increase of n_{ss} in the lower part of the bandgap. Furthermore, we see that the annihilation of holes does not anneal the interface states already generated. It is thermal energy that does the annealing.

The second experiment we performed was photoinjecting electrons immediately after the high field stressing (7.5 MV/cm) at 90°K. The injection was terminated when the shift of the C-V curves was saturated. Figure 3.13 shows the results after the sample was warmed up. Curve 1 shows n_{ss} after the sample had been held at 66°C for 1 hour. Curve 2 shows n_{ss} after another hour at 96°C, and Curve 3 shows n_{ss} after another hour at 120°C. Not surprisingly, these curves show much fewer interface states than any of the other samples.

3.4. Discussion

Holes and thermal energy are the key factors in generating interface states. Holes may be introduced either by ionizing radiation or by high field stress. However, these are not necessarily the only ways to create interface states. Very possibly, the high electric field itself may have some intrinsic effect on the generation of interface states. The generation processes probably involves an electrochemical reaction with the holes playing the role of setting a charged atomic or molecular species free.

We do not observe any one definite energy level at which the n_{ss} function shows a characteristic peak. The shift that we observed in the peak of the n_{ss} function may be the consequence of two different effects. First, we have a slow generation process, very possibly a diffusion-controlled process, which may have an activation energy that depends on the energy at which the hole is located in the bandgap. To complete a process with a comparatively large activation energy might take months at room temperature but

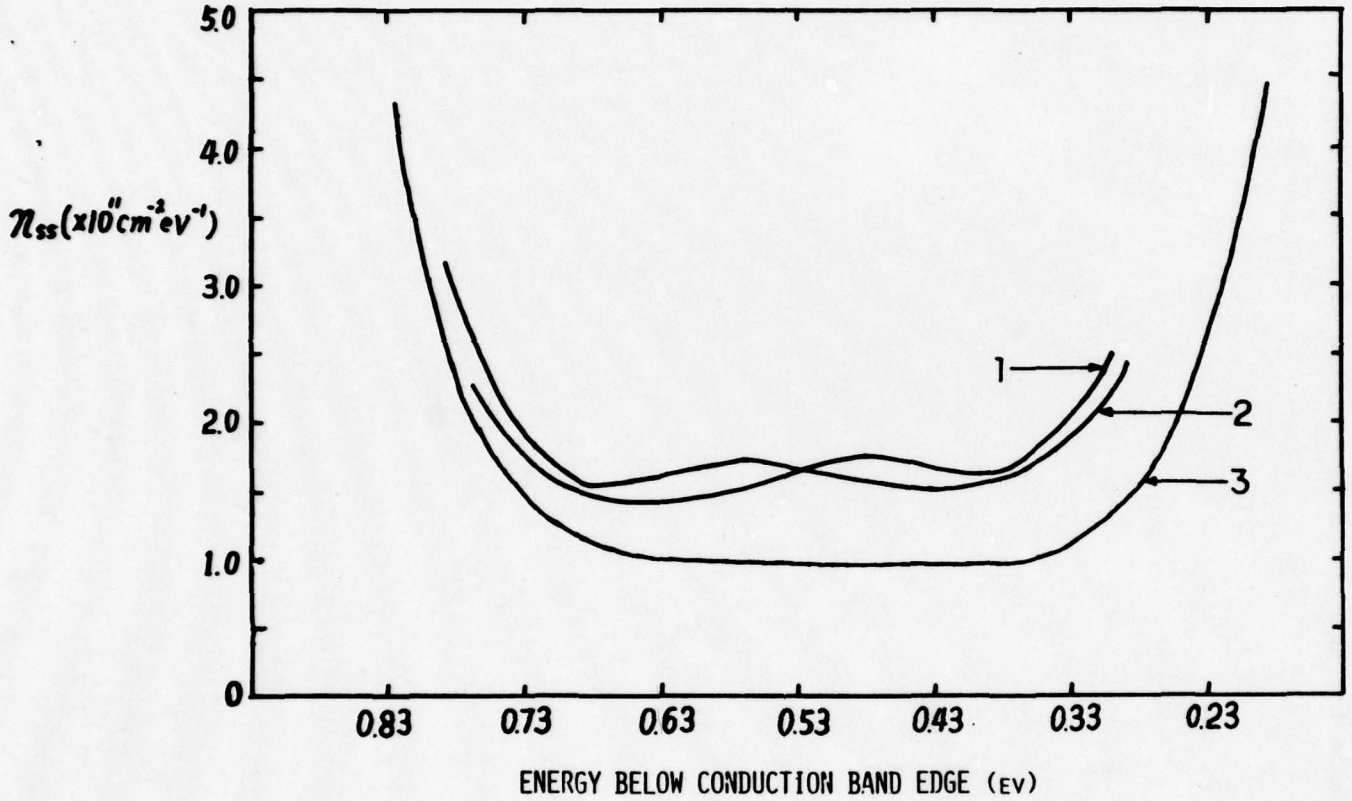

Fig. 3.13. Energy distribution of interface states of a sample that had been high-field stressed at 90°K for 15 mins with 7.54 MV/cm, followed by a photoinjection of 1.0 x 10^{14} electrons/cm^2 into oxide, after which the sample was warmed. Curves 1, 2 and 3 were obtained after the sample had been held for one hour each at 66°C, 96°C and 120°C.

only a few hours at elevated temperature. Second, we have an annealing process which requires thermal energy. The rate of annealing will depend on the temperature and may also depend on the energy level at which the interface state is located. A peak may be built up where the competition between these two processes is favorable for generation as compared with annealing.

4. CHARACTERISTICS OF THE CHARGE TRAPPING IN CVD Al_2O_3 ON SILICON
(S. S. Li collaborating)

4.1 Introduction

In this chapter we present the results of an investigation of charge trapping in the aluminum-oxide insulators of Metal-Al_2O_3-Si (MAS) capacitors. The electron-trap energy spectrum and the spatial distribution of the traps have been studied previously by several workers. Mehta et al[21] photoinjected electrons into Al_2O_3 from the silicon substrate. The results of subsequent photodepopulation indicated that the centroid of the trapped charges released by 2.60 eV photons was located at 0.30 d from the oxide-silicon substrate interface, where d is the thickness of the insulator. Powell and Hughes,[22] in their studies of the electron trapping in MAS structures, found evidence that the trapped electrons tended to be strongly localized near the Si-Al_2O_3 and Metal-Al_2O_3 interfaces. More detailed photodepopulation studies of the electron trapping characteristics were conducted by Harari and Royce[23] and by Harari.[24] They observed five different trapping levels with energy depths located between 2.2 eV and 4.4 eV below the conduction band. At liquid nitrogen temperature, the trapped charges were essentially uniformly distributed.

In order to study current injection and high field effects in the oxide, further knowledge about the trap characteristics is required. Therefore, in this work, the photodepopulation technique was adopted to study the effect of temperature and the effect of electric field strength on the trapped charge. Estimation of the position of the space-charge centroid by the photo I-V method provided additional evidence regarding the location of the electron traps. An analysis of the electron capture process was also developed. This provides an unambiguous criterion for determining whether displacement current has to be taken into account in deducing the capture cross section of the traps. The effects of thermal anneal on the space charge was also investigated.

4.2. Description of Samples

Our MAS capacitors were fabricated at Bell Laboratories by courtesy of David Boulin. The insulator was 900°C pyrolytically grown

Al_2O_3 on both n-type and p-type (100) silicon substrates having resistivities in the 4-6 Ω-cm range. Both gold and aluminum field plates were evaporated on the surface of the oxide. The oxide thicknesses were in the range from 450Å to 1086Å. The semitransparent gold field plates ("gates") had a sheet resistivity of 5Ω/□. The sheet resistivity of the semitransparent aluminum plates ranged from 10Ω/□ to 22Ω/□. Samples used for the thermal anneal had thick (∿1000Å) aluminum gates. Table I summarizes the types of samples that we used in these investigations.

4.3. Studies of Electron Trapping by Optical Technique

4.3(A). Analysis and Experimental Setup

When the metal-aluminum oxide-silicon structure is exposed to photons that penetrate the metal, several processes can occur in the insulator: (a) the electrons with trapping energy within hν of the conduction band edge can be excited into the conduction band by absorption of photons; (b) electrons can be photoinjected from the negative electrode into the oxide, then be captured; and (c), electrons can be photoexcited from the Al_2O_3 valence band into traps. In this work, Processes (b) and (c) are shown to make negligible contributions in comparison with Process (a).

The traps can be populated by capture of electrons that are introduced into the oxide by either internal photoemission or high field injection.[26] During the subsequent optical depopulation ("bleaching") process,[26-28] the gate was biased negatively so that the photoreleased charges would be driven out of the oxide and into the substrate. (Here the first-order approximation is made that charge retrapping can be neglected). The external current induced by the detrapped charges was integrated by a Keithley 602 electrometer operating in the coulombic mode. The photocurrent level eventually became very small and approached the dark current level. The net amount of charge contributed by the optical depopulation was obtained by subtracting the charge component contributed by the dark current. C-V measurements were made both before and after each photodepopulation step to obtain the voltage shift resulting from the photoreleased charges. Since the insulator studied contains a very high concentration of electron traps, any flow of charge carriers through the oxide will be accompanied by a build-up of space charge. It is thus necessary that the measured current be determined from both the particle current and displacement current, i.e.,

TABLE I - DESCRIPTION OF TEST SAMPLES

	Substrate	Oxide Thickness	Field Plate
P-900	n-type	450Å	Al, ~ 100Å
P-971,972	p-type	881Å	Au, 5Ω/□ ~150Å
Dots A,B,C	n-type	1089Å	Au, 5Ω/□ ~150Å
P-969	p-type	474Å	Au, 5Ω/□ ~150Å
Dots E,F	p-type	881Å	Au, 5Ω/□ ~150Å

$$J_{ext} = J_{out}(x = d) + \frac{dD}{dt} \tag{4.1}$$

where $J_{out}(x = d)$ is the particle current which drifts through the metal-insulator interface and D is the electric displacement at this interface. The origin of x is taken at the oxide-substrate interface and d is the thickness of the oxide. According to Gauss's law, dD/dt can be replaced by dQ/dt, where Q includes the total amount of charge stored in the insulator and in the silicon substrate, on or near the interface.

$$J_{ext} = J_{out}(x = d) + \frac{dQ}{dt} \tag{4.2}$$

The transport of the photoreleased electrons through the metal-Al_2O_3 interface can be prevented during the photodepopulation process by applying a negative field strong enough so that no positive field exists at the front surface, i.e.,

$$V \geq \frac{Q_T}{\varepsilon} \bar{x}_T \tag{4.3}$$

where $\bar{x}_T$ is the location of the centroid of the total charge distribution and Q_T is the total charge. Then we have

$$J_{ext} = \frac{dQ}{dt} \tag{4.4}$$

Furthermore,

$$J_{ext} = \frac{dQ_D}{dt} \frac{\bar{x}}{d} \tag{4.5}$$

where $\bar{x}$ is the centroid of the photoreleased charges,
and Q_D is the photoreleased charges.

After integration of Eq. (4.5), we have

$$\Delta Q_{ext} = \Delta Q_D \frac{\bar{x}}{d} \tag{4.6}$$

The change in flatband voltage caused by the released charge is given by $\Delta V_{FB} = (d - \bar{x})\Delta Q_D/\varepsilon$. Therefore,

$$\frac{\Delta Q_{ext}}{\Delta V_{FB}} = C_{ox} \frac{\bar{x}/d}{1-\bar{x}/d} \qquad (4.7)$$

The total externally collected charge and the change in flatband voltage are measurable quantities; thus, the centroid of the released charge can be determined by applying Eq. (4.7).

4.3(B). High Field and Photo Depopulation

The samples used in this experiment were MAS capacitors with insulator thicknesses of 881Å, 474Å, and 1089Å. Semitransparent gold field plates with resistivity of 5Ω/□ (∿150Å) were evaporated on the surface of the insulator. Owing to the large barrier height between the gold and the Al_2O_3 (4.1 ± 0.1 eV),[29,30] it is possible to use photons with energies up to 4 eV to photodepopulate the trapped electrons without photoinjecting electrons into the oxide. Two capacitors were used as control samples: P-900 and P-971, whose characteristics were described in Table I. Both of these samples initially had positive flatband voltages (≈ 2.7 - 2.8 V) which we tried to reduce or eliminate by photodepopulation. We short circuited the field plate of Capacitor P-900 to its substrate and used photons with energies of 2.2 eV, 2.5 eV and 3.0 eV in successive steps of two hours each. This resulted in only an 0.2 V flatband voltage shift (positive). Capacitor P-971 was biased at -1.36 MV/cm (-12 V) and was illuminated by 4 eV photons for an hour, but no flatband voltage change was detected. These results indicate that the initial negative charge is stored deeply.

The experimental procedures and results for Capacitor P-972 are given in Table II. By applying the high positive field to the sample, electrons were field injected into the oxide to fill the traps, and resulted in a large positive flatband shift. The reversed field discharged many of the electron traps and reduced V_{FB} considerably. As will be shown in a later section, the reduction in flatband voltage was due mainly to the tunneling of electrons from traps located close to the interface where a high concentration of shallow electron traps exists. For the photodepopulation, we started with a photon energy of 2.5 eV and increased the energy in increments of 0.2 eV, ending at 4.0 eV. A complete photodepopulation

Table II. The charging and discharging characteristics of MAS capacitor P-972. The flatband voltage was measured immediately after field stress or photodepopulation. The thickness of the oxide was 881Å.

P-972	V_{FB}
Fresh dot	3.0volts
+38v, 50minutes	23.5volts
-12v, 75minutes	16.8volts
After Photodepopulation	5.3 volts

operation was performed on Capacitor P-972. During the run, the external current was not collected, but the results of the consecutive flatband voltage shifts with respect to time are shown in Fig. 4.1. The charge detrapping is described by the following equation:[31,33,34]

$$\frac{dn_t}{dt} = -S(x)\sigma_p n_t(x,t) \qquad (4.8)$$

where S(x) is the photon flux at position x and σ_p is the electron photoionization cross section which is assumed to be spatially independent. Integrating over the time, we have:

$$n_t(x,t) = n_t(x,0)\ \exp(-\sigma_p S(x)t). \qquad (4.9)$$

The total amount of detrapped charge is obtained by integrating over the whole oxide thickness:

$$Q_d(t) = q\int_0^d [n_t(x,0) - n_t(x,t)]\ dx. \qquad (4.10)$$

If optical interference[35] is not important, the amount of detrapped charge can be expressed as

$$Q_d(t) = Q_t(0)[1 - \exp(-\sigma_p\ St)] \qquad (4.11)$$

where $Q_t(0)$ is the amount of charge trapped at t = 0.

A slow photodepopulation process indicates either that the light intensity S is weak or that the photoionization cross section σ_{op} is small. In making measurements to determine the energy profile of the trapped electrons, the resolution of the UV light was adjusted to 45Å for photons with energy greater than 3 eV, and to 80Å for photons less than 3 eV. To measure the charge centroid, the width of the exit slit of the monochromator was doubled to improve the charge detrapping rate. The UV source used was a xenon 150W lamp with B&L high-intensity monochromator.

4.3(C). Effect of Temperature on the Space Charge

The effect of temperature on the spatial distribution and energy spectrum of the trapped charges will now be discussed. Three n-type Au-Al_2O_3-Si capacitors with 1089Å oxides were utilized in these studies. The experimental

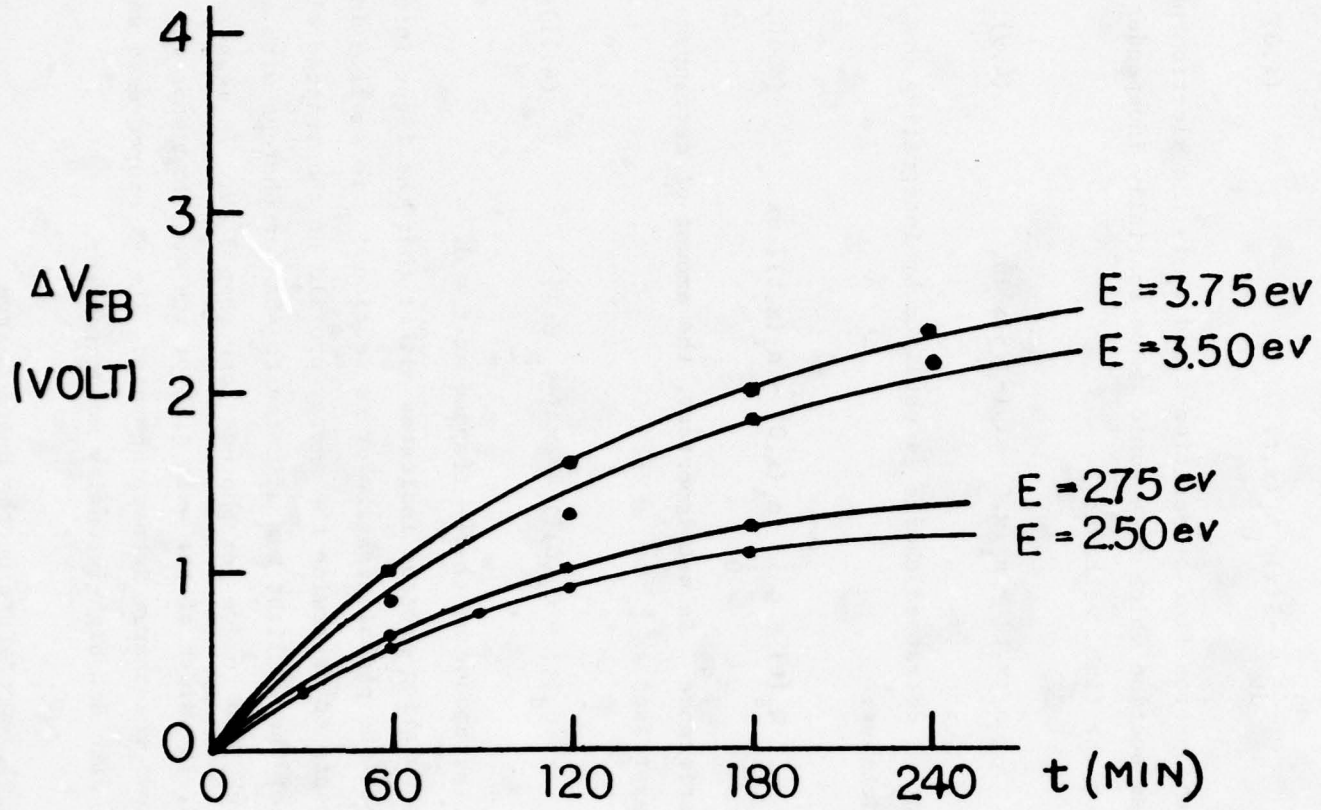

Fig. 4.1. The change in flatband voltage as a function of time, obtained by photobleaching the charged traps of Capacitor P-972 with monochromatic light. The first photodepopulation was done with light having a photon energy of 2.5 eV. The energy was incremented in 0.25 eV steps, and the highest energy used was 4.0 eV. The curves were drawn by eye for a "best fit." Only four of the curves are exhibited.

procedures and results obtained on Dots A, B and C are shown in Table III. Dot A was subjected to a moderate positive gate bias and was illuminated by 5 eV photons for 20 minutes. Following this, the positive bias was increased and the illumination was maintained for 30 additional minutes. The positive bias was then increased (average field 4.4 MV/cm) and held for 5 minutes without illumination. The photo and field injection of electrons, accompanied by trapping, increased the flatband voltage from 4.3 volts to 30.1 volts. The sample was then stressed with a negative bias of -14V for one hour. This resulted in a reduction of flatband voltage to 23.6 volts. A complete photodepopulation run was then conducted by exposing the MAS structures to high resolution UV photons, starting at 2.0 eV and incrementing by 0.2 eV up to a maximum of 4.0 eV. Each step was held until the change in flatband voltage was essentially complete. The resulting energy profile of the released charge as a function of photon energy is shown in Fig. 4.2.

After the photodepopulation, the flatband voltage was found to have been reduced to 7.2 volts, indicating that most of the trapped electrons had been located at optical energies in the upper half of the band gap. As can be seen in Fig. 4.2, the optical energies of the trapped electrons were distributed continuously from shallow levels to deep levels with three energy peaks locacted at 2.8 eV, 3.2 eV and 3.6 eV. The location of the peaks is similar to the A, B, and C bands observed by Harari and Royce.[23,24] A small amount of shallowly trapped charge with energies less than 2.2 eV is also noted.

In an attempt to investigate the shallow trapped charge, further experiments were performed at liquid nitrogen temperature. Dot B, which had a 1089Å oxide, was cooled to 95°K. In a set of operations preceding those shown in Table III, the sample was biased to +15 volts and internal photoemission was used to photoinject electrons so as to populate the electron traps. Then, to probe the shallow traps, the sample was stressed at +20 volts and was successively exposed to 2.0 eV and 2.25 eV photons for 3 hrs each. C-V measurements indicated that there were respectively 0.9 volt and 0.8 volt decreases in flatband voltage after each illumination. Thus, appreciable concentrations of shallow traps exist within the oxide.

Dot A, 300°K	V_{FB}
Fresh dot	4.3volt
+15 volt, +38 volt } 5ev illumination & +48 volts, 5minutes	30.1 volts
-14 volts, 60minutes	23.6volts
After Photodepopulation	7.2volts

Dot B, 95°K	V_{FB}
Fresh dot	5.2volts
+38volts, 4.8ev photoinjection	32.6volts
-14volts, 75minutes	26.0volts
After Photodepopulation	9.6volts

Dot C, 300°K	V_{FB}
Fresh dot	4.2volts
+38volts, 4.8ev photoinjection	28.9volts
-14volts, 75minutes	21.0volts
After Photodepopulation	7.7volts

Table III. The charging and discharging characteristics of three MAS capacitors denoted as Dots A, B and C. The flatband voltage was determined from C-V measurements made immediately after each field stress or photodepopulation step. The thickness of the oxide was 1089Å.

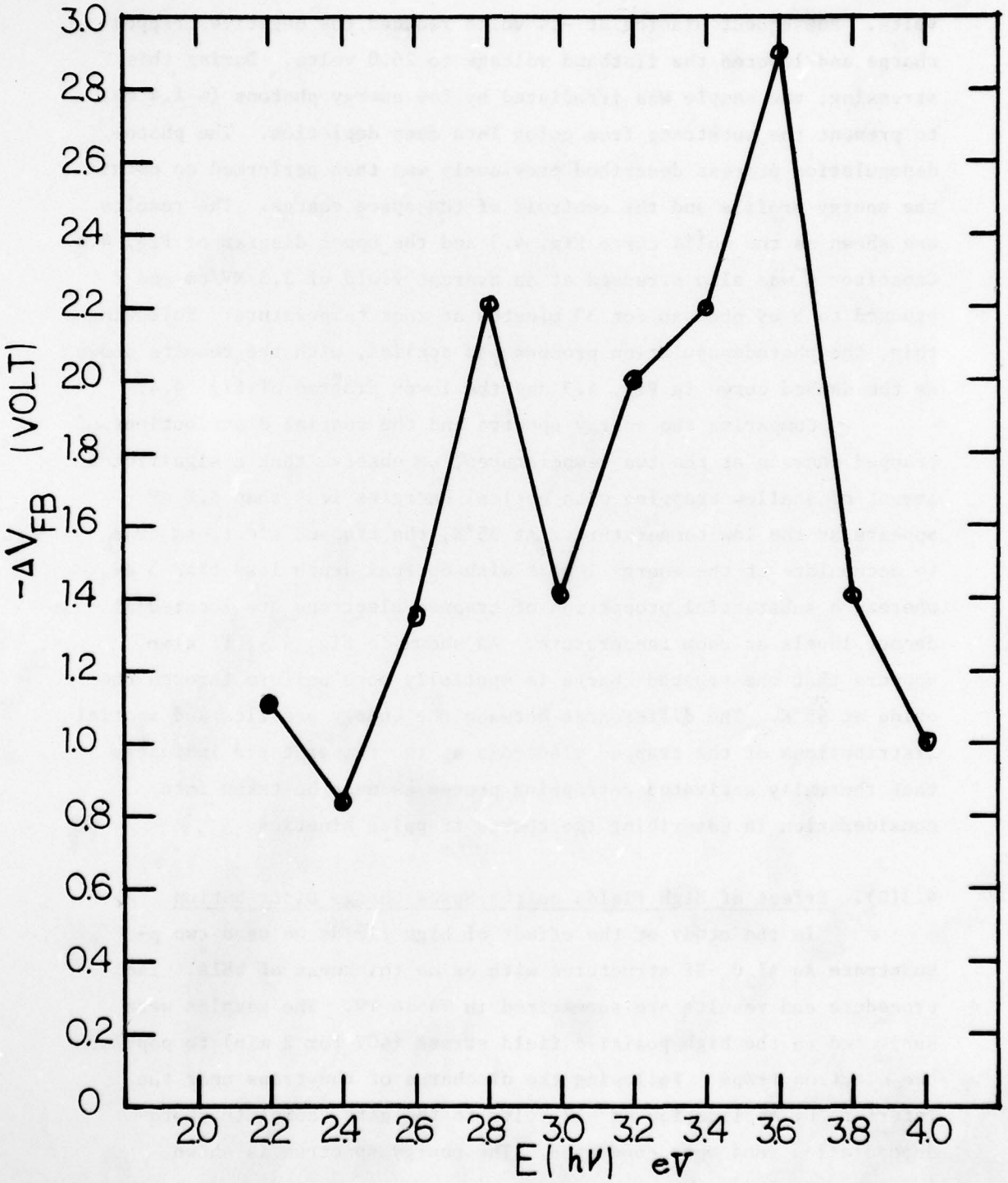

Fig. 4.2. Plot of the flatband voltage change ΔV_{FB} versus the photon energies, E = hν, obtained by irradiating the MAS sample with high-resolution UV light.

As shown in Table III, the sample was then stressed at +38 volts and was simultaneously exposed to 4.8 eV photons for 30 min. The resulting injection of electrons caused the flatband voltage to shift to +32.6 volts. Subsequent biasing at -14 volts reduced the negative trapped charge and lowered the flatband voltage to 26.0 volts. During this stressing, the sample was irradiated by low energy photons ($\sim$ 1.4 eV) to prevent the substrate from going into deep depletion. The photodepopulation process described previously was then performed to obtain the energy profile and the centroid of the space charge. The results are shown as the solid curve Fig. 4.3 and the upper diagram of Fig. 4.4. Capacitor C was also stressed at an average field of 3.5 MV/cm and exposed to 5 eV photons for 30 minutes at room temperature. Following this, the photodepopulation process was applied, with the results shown as the dashed curve in Fig. 4.3 and the lower diagram of Fig. 4.4.

Comparing the energy spectra and the spatial distributions of trapped charges at the two temperatures, we observe that a significant amount of shallow trapping with optical energies less than 3.2 eV appears at the low temperature. At 95°K, the trapped electrons tend to accumulate at the energy levels with optical depth less than 3 eV, whereas a substantial proportion of trapped electrons are located at deeper levels at room temperature. As shown in Fig. 4.4, it also appears that the trapped charge is spatially more uniform through the oxide at 95°K. The differences between the energy profiles and spatial distributions of the trapped electrons at two temperatures indicates that thermally activated detrapping processes must be taken into consideration in describing the charge trapping kinetics.

4.3(D). Effect of High Fields on the Space Charge Distribution

In the study of the effect of high fields we used two p-substrate Au-Al_2O_3-Si structures with oxide thickness of 881Å. The procedure and results are summarized in Table IV. The samples were subjected to the high positive field stress (40V for 2 min) to populate the electron traps. Following the discharge of the traps near the interface by application of -12 volts to the gate, complete photodepopulation runs were conducted. The energy spectrum is shown

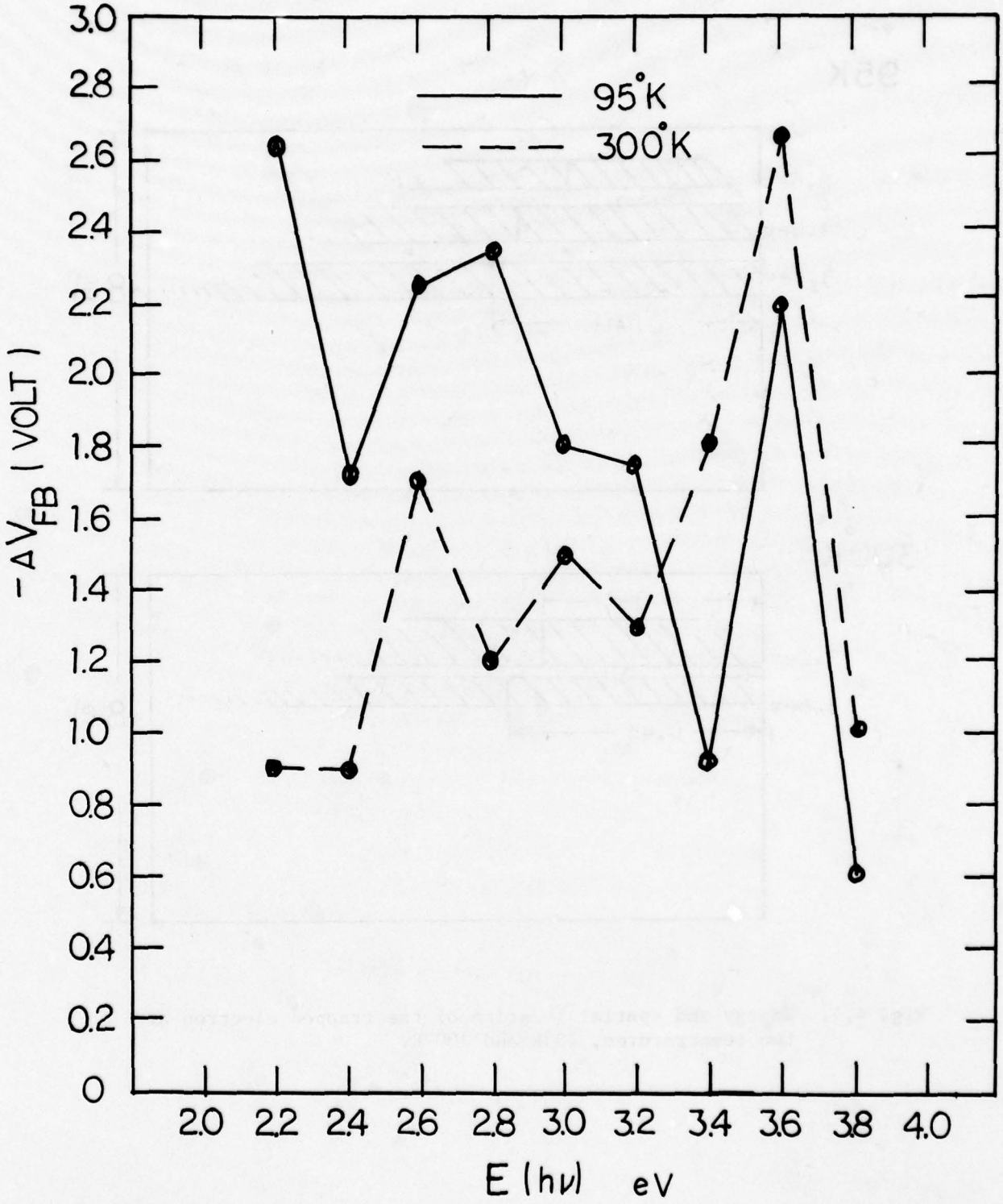

Fig. 4.3. Effect of temperature on the energy spectrum of the trapped electrons.

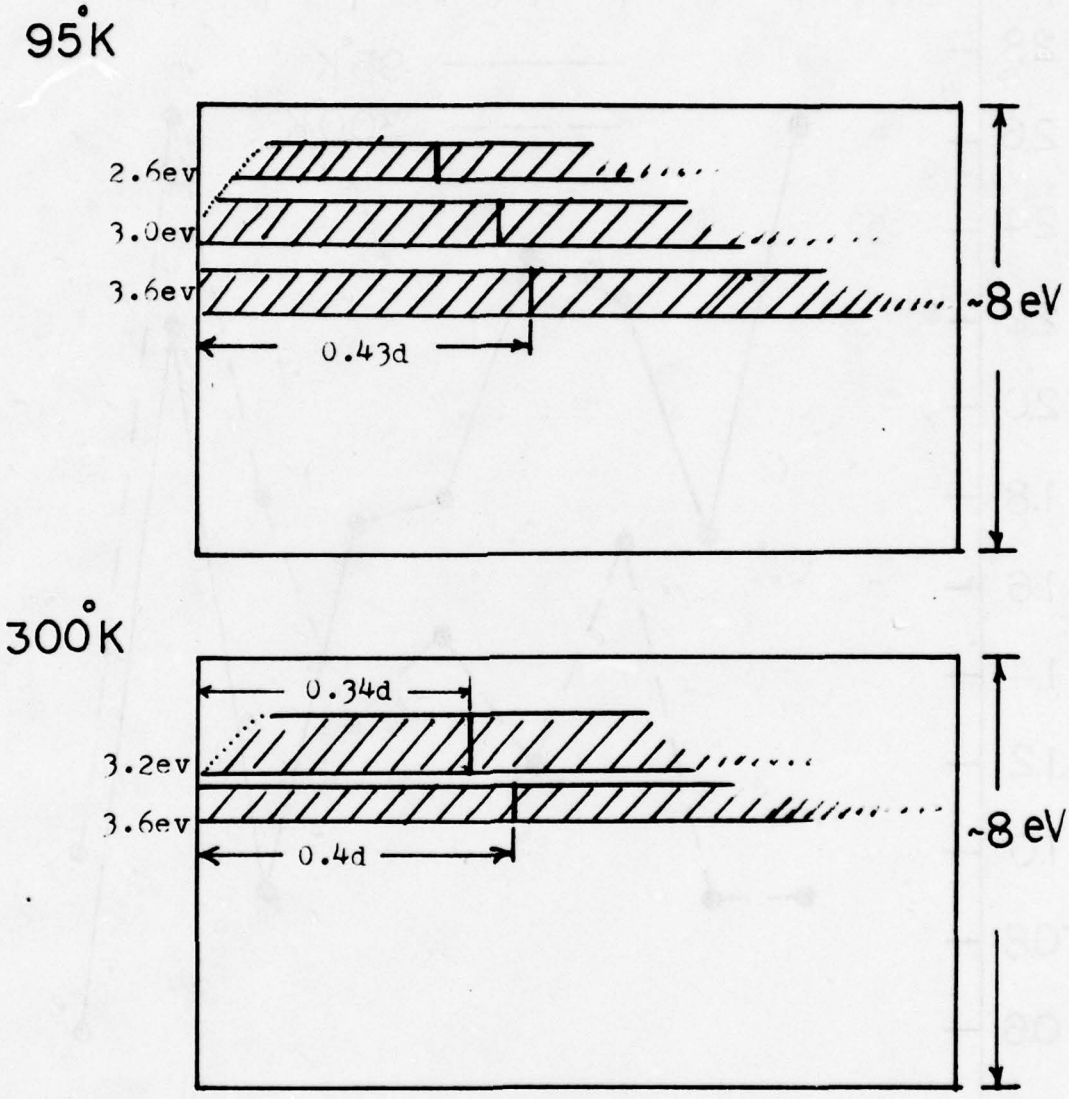

Fig. 4.4. Energy and spatial location of the trapped electron at two temperatures, 95°K and 300°K.

Table IV. The charging and discharging characteristics of Capacitors E and F. The C-V measurements were made immediately after each field stress or photodepopulation step. The thickness of the oxide was 881Å.

	V_{FB}	
	# 1	# 2
Fresh dot	2.6volt	3.0volt
+40volt, 2minutes	22.5volt	(V_{FB} not measured)
-12volt, 75minutes	15.3volt	-
-12volt, 11hours	-	16.5volt
After Photodepopulation	3.45volt	4.6volt

in Fig. 4.5, which shows three peaks located around 2.5 eV, 3.0 eV and 3.6 eV. The centroid of these trapping levels is located between 0.27 d and 0.4 d. The results again indicate that when samples are under high field stress at room temperature, the trapped electrons extend throughout the bulk of the oxide. The site with a high concentration of trapped electrons is located close to the injecting electrode. By comparing the energy profiles of the two capacitors (Fig. 4.5) it appears that one of the capacitors has a higher concentration of shallow traps than the other. The influence of this on the electronic properties of the samples will be discussed in a later section.

4.3(E). Estimation of Position of the Trapped-Charge Centroid by the Photo I-V Method

We also estimated the position of the trapped-charge centroid by the photo I-V technique which was proposed by Powell and Berglund[31] and by Dimara.[36]

The sample used in this experiment was p-substrate with oxide thickness of 967Å. The initial flatband voltage was measured to be 1.6 volts. Photoinjection of electrons was then performed to fill up the traps while the bias was maintained at an average field of -2.05 MV/cm for an hour. This shifted the flatband voltage to 10.6 volts. The photocurrent after an hour of photoinjection was observed to decay very slowly. Data on the photocurrent versus the gate voltage was then taken by varying the bias from -26 volts to -13 volts. A subsequent C-V measurement indicated an 0.5 volt decrease in flatband voltage, this being small in comparison with the total flatband voltage. The photo I-V plot is shown in Fig. 4.6. The applied voltage ranged over only negative values because the application of positive fields would have redistributed the trapped charges.

According to Powell and Berglund's analysis,[31] if the negative charges are uniformly distributed in the bulk of the oxide, the photo I-V curve of the charged capacitor should be parallel to that of the uncharged sample. However, a true photo I-V curve was difficult to obtain for our uncharged sample, for many of the photoinjected electrons were trapped in the many empty traps and the external current was

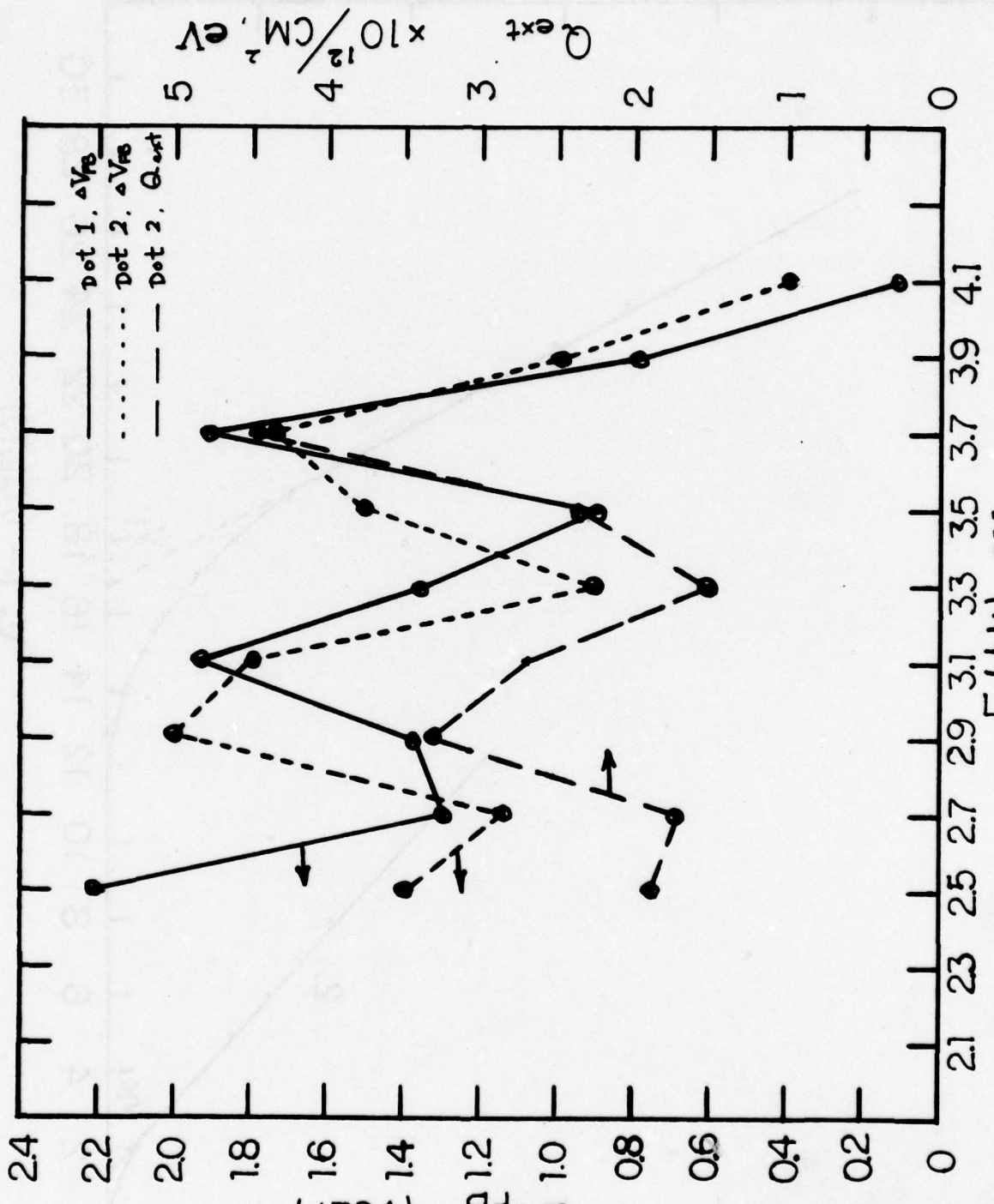

Fig. 4.5. Plots of flatband voltage change and, for one of the capacitors, of externally collected charge, obtained by photodepopulating two MAS capacitors at room temperature.

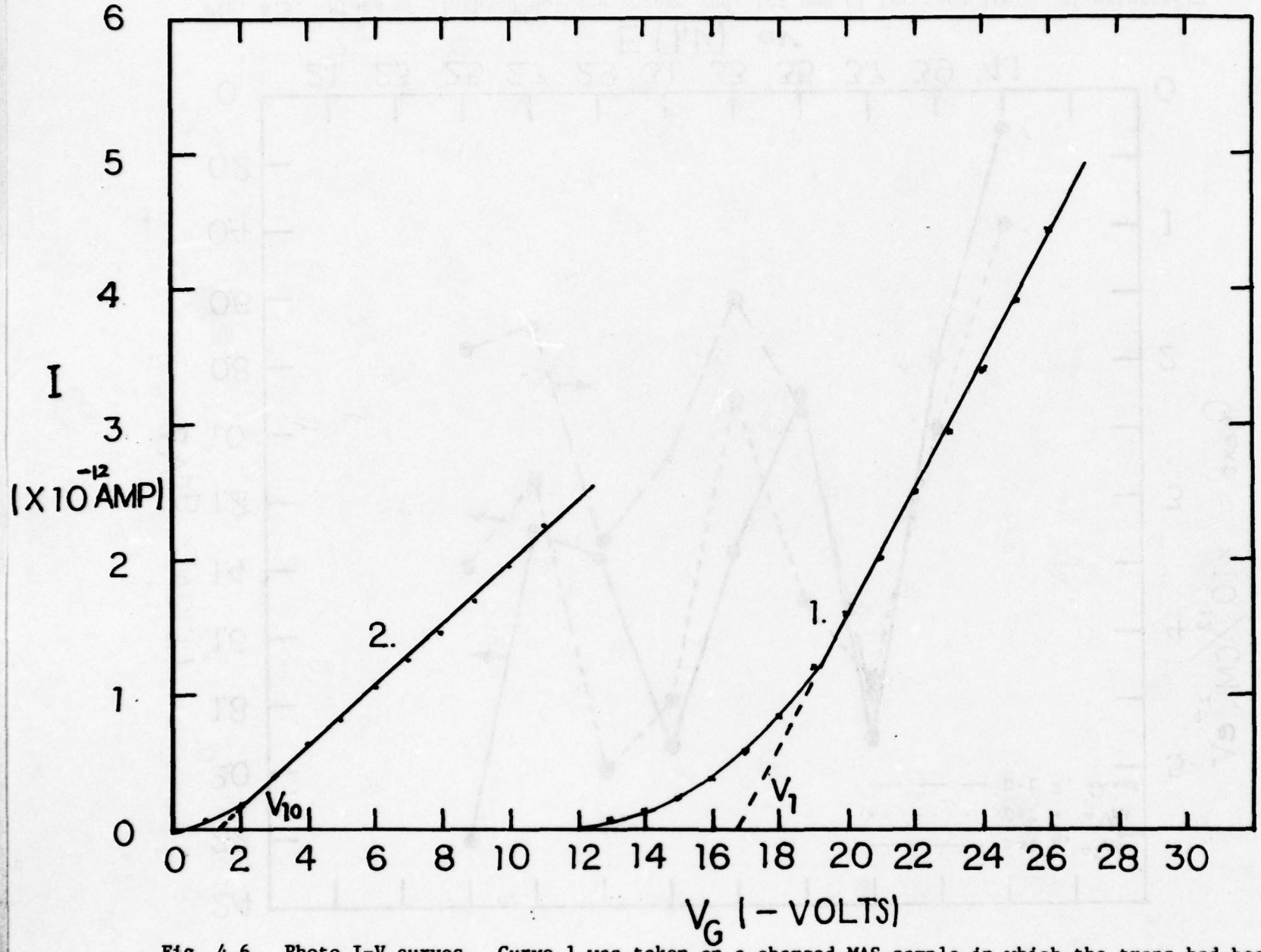

Fig. 4.6. Photo I-V curves. Curve 1 was taken on a charged MAS sample in which the traps had been populated by internally photoinjecting electrons from the negatively biased field plate. Curve 2 was taken on an uncharged MAS capacitor.

correspondingly reduced (Curve 2 of Fig. 4.6). The photo I-V curve of our charged sample (Curve 1 of Fig. 4.6) showed a tail at the bottom. This may have been caused by laterally nonuniform charge trapping near the front surface. The appropriate relations are:

$$\Delta V = V_1 - V_{10} = \frac{\bar{x} Q}{\epsilon} \tag{4.12}$$

where V_1 and V_{10} are obtained as shown in Fig. 4.6,

and $$V_{FB} = \frac{d - x}{\epsilon} Q \tag{4.13}$$

If we take V_{10} to be 1.2 volts, the centroid is computed to be around 610 Å from the silicon-insulator interface, namely at 0.63 d. This provides further evidence that our Al_2O_3 traps substantial amounts of charge in the bulk, not just near the interface. In connection with the location of the centroid, it should be observed that in this experiment the electrons were injected from the metal field plate.

4.3(F) Comment

Before the photoreleased charge is swept out of the oxide by the external field, it can be recaptured into traps. If the recaptured electrons are located in an energy range which is shallower than the photon energy, the charge can be detrapped again. Denote by Q_t the total amount of charge that originally had optical depths less than $h\nu$. Then Q_t can be written as the sum of Q_1, the number of trapped charges depopulated by $h\nu$ and swept out of the oxide, and Q_2, the number of trapped charge detrapped by photons of energy $h\nu$ and retrapped into deep levels. The original centroids of Q_t, Q_1 and Q_2 will be denoted by $\bar{x}_t$, $\bar{x}_1$ and $\bar{x}_2$ respectively. After photodepopulation, the centroid of Q_2 shifts to $\bar{x}_2'$. Therefore, the actual amount of charge measured in the external circuit, Q_{actual}, is

$$Q_{actual} = Q_1 \frac{\bar{x}_1}{d} + \frac{Q_2}{d} (\bar{x}_2 - \bar{x}_2') \tag{4.14}$$

whereas without retrapping the collected charge would have been

$$Q_{coll} = \frac{Q_t}{d} \bar{x}_t \tag{4.15}$$

The actual measured flatband voltage change is equal to

$$\Delta V_{FB(actual)} = \Delta V_{FB} - \Delta V_{FB'} = \frac{Q_t(d-\bar{x}_t)}{\epsilon} - \frac{Q_2(d-x_2')}{\epsilon}$$

The actual amount of charge collected in the external circuit is

$$Q_{actual} = Q_1 - \Delta V_{FB(actual)} C_{ox}$$

and

$$\frac{Q_{actual}}{\Delta V_{FB(actual)}} = C_{ox}\left(\frac{Q_1}{C_{ox}\Delta V_{FB(actual)}} - 1\right) \qquad (4.16)$$

If $Q_1 = m\, Q_t$, where $0 \leq m \leq 1$, Eq. (4.18) can be written as

$$\frac{Q_{actual}}{\Delta V_{FB(actual)}} = m\, C_{ox}\left(\frac{d}{d - \bar{x}_t - (1-m)(d - x_2')} - 1\right) \qquad (4.17)$$

The measured centroid therefore is given by

$$\bar{x}_{t(measured)} = \frac{\bar{x}_t}{m} + x_2'(1 - 1/m) \qquad (4.18)$$

When x_2' is larger than $\bar{x}_t$, the measured centroid is smaller than the true centroid (nearer the Si-oxide interface) and vice versa.

During the photodepopulation process, substantial proportions of deep traps are already occupied, and the opportunity for electrons to be recaptured into these levels is quite limited. The retrapping of photoreleased carriers is more likely to occur into the relatively shallow levels where detrapping can eventually take place by long-time bleaching. The value of m is therefore expected to be close to unity.

4.3(G). Trapping and Detrapping Kinetics Within the Oxide

Further studies were attempted to investigate the effect of temperature on the trapped-charge spatial distribution and energy spectrum.

Sample P-969 (with an oxide thickness of 474Å) was cooled down to 93°K. The electron traps were then populated by subjecting the device to an average field of 5.0 MV/cm (+24 volts) for 20 minutes. After the field injection of electrons, V_{FB} was found to have increased from 2.5 volts to 12.5 volts. The sample was subsequently biased to an average field of -2.9 MV/cm for 50 minutes, which resulted in the reduction of flat-band voltage to 7.9 volts. Following 270 minutes of photodepopulation by 2.75 eV photons, the flatband voltage shifted to 7.25 volts. The external bias was then held at 8.5 volts and the sample was warmed up to room temperature. The C-V measurement made at room temperature indicates that there was a 1.25-volt flatband-voltage decrease. The minimum amount of trapped charge lost during the warmup process was computed to be $1.4 \times 10^{12}/cm^2$ (in which the effect of interface states had been subtracted). As reported previously, this observation suggests a temperature-activated field-dependent hopping mechanism within the oxide, together with Poole-Frenkel barrier-lowering.

A photodepopulation experiment, also, was performed on sample P-969. The MAS structure was first exposed to 5 eV photons while biased at the relatively low (average) field of 2.75 MV/cm for 30 minutes to fill the traps with electrons. Then a complete photodepopulation run was conducted, resulting in the energy profile shown by the dashed curve in Fig. 4.7. The sample was next subjected to high field stress of 4.6 MV/cm (average field) for 30 minutes. The photodepopulation procedure was then repeated. The flatband voltage changes as a function of photon energies as shown by the solid curve of Fig. 4.7. Comparison of two energy profiles indicates that a larger proportion of electrons are trapped in shallow levels if the traps are populated by photo-injection at a low field at room temperature.

In order to gain additional information regarding the influence of high fields on the electrons trapped in shallow levels, Capacitor E, which had an 881Å oxide, was subjected to the comparatively large bias of 38 volts for only 2 minutes. After this stressing, the flatband voltage was found to have shifted from 3.1 volts to 21.5 volts, as shown in Table V. The sample was then held at -12 volts for 75 minutes

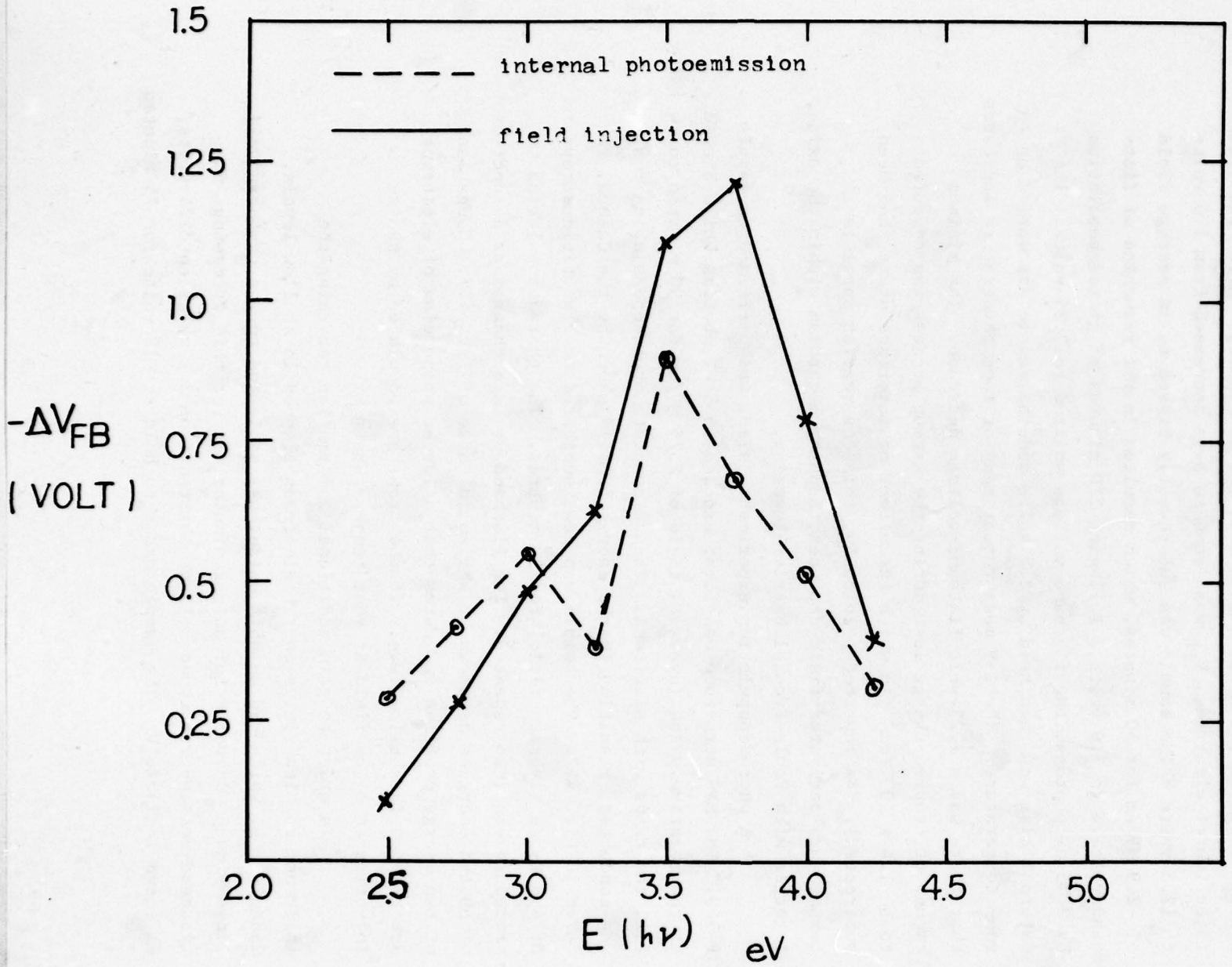

Fig. 4.7. Plot of the flatband voltage shift as a function of photon energy for MAS capacitor. The dashed curve exhibits the energy profile of the electrons in traps populated by internal photoemission at relatively low field, while the solid curve shows the energy profile of electrons in traps populated by high field injection.

Table V. The charging and discharging characteristics of Capacitors E and F. The flatband voltages were measured immediately after each stress or photodepopulation step. The oxide thickness was 881Å.

	V_{FB}	
	Sample E	Sample F
Fresh Dot	3.1volts	2.8volts
+40volts, 2min.	—	22.5volts
+38volts, 2min.	21.5volts	—
-12volts, 75min.	15.0volts	15.6volts
2.5ev, 4hrs photodepopulation	12.7volts	13.8volts
(centroid	272Å	240Å)
+40volts, 90min.	—	24.5volts
+38volts, 30min.	23.5volts	—
-12volts, 75min.	17.2volts	18.1volts
2.5ev, 4hrs photodepopulation	15.1volts	16.1volts
(centroid	247Å	209Å)

to discharge the traps close to the interface. The sample was then illuminated with 2.5 eV photons for 4 hours to discharge the shallow traps. The flatband voltage was found to have changed from 15.0 volts to 12.7 volts, a change of -2.3 volts, and the centroid of the shallowly trapped electrons was found to be 272Å from the silicon-oxide interface (see Table V). This result is to be contrasted with the one obtained by populating the traps again at 38 volts but for the longer time of 30 minutes. After discharge of the traps near the interface by application of -12 volts for 75 minutes, the flatband voltage was found to be greater (17.2 volts) than in the corresponding step of the previous experiment. After photodepopulation with 2.5 eV photons, the flatband voltage was found to have changed by -2.1 volts, which was proportionately smaller than in the corresponding step of the previous experiment, and the centroid of the shallowly trapped charge was found to be closer to the silicon-oxide interface: at 247Å. Similar results, as shown in Table V, were obtained on Sample F when it was subjected to a similar set of tests. We shall interpret these results in the discussion below.

Owing to the high concentration of electron traps within the oxide, the injected electrons have very high probabilities of being captured without traversing long distance through the oxide. At liquid nitrogen temperature, the thermally activated detrapping processes are highly suppressed so that the emission time constant[32] for electrons captured into shallow levels is much longer. The relatively higher concentration of electrons accumulating in the shallow levels with optical depths less than 3.0 eV indicates either that there are more shallow traps than deep ones in the oxide or that the capture cross section of the shallow traps is larger than that of the deep ones. With regard to the large amount of electron traps at optical depths less than 2.2 eV, these provide potential wells in the energy barrier to assist the electrons in the conduction band of the substrate to undergo trap-assisted tunneling.[8,37,38] The centroid of the shallowly trapped electrons is located at 0.30 d - 0.36 d from the substrate-insulator interface, whereas the centroid of the deep levels is measured to be 0.38 d to 0.44 d from the interface. Electron traps are therefore seen to extend throughout the oxide. When the traps have captured electrons, the energy bands are bent convex upward, and the electric

field near the positive electrode is greatly enhanced. In our operation of high-field injection to populate the traps, this electrode is the metal field plate. It is possible that at these high fields, some conduction electrons may attain enough energy to release trapped electrons by impact ionization. This process would operate even at liquid nitrogen temperature. Shallowly trapped electrons also have higher possibilities of tunneling out of traps. Therefore we would expect to have fewer shallowly trapped electrons near the field plate, i.e., the centroid of the shallowly trapped electrons should be nearer the silicon-oxide interface, as we have seen in Table V.

As the temperature was increased toward room temperature, the trapped electrons were observed to undergo detrapping processes. Comparing Curve 2 with Curve 1 in Fig. 4.3, we observe that a high concentration of trapped electrons occupied the deep levels while the number of shallowly trapped electrons with energies around 2.2 eV decreased significantly. Thermally activated processes, including thermally activated field-dependent hopping and Poole-Frenkel emission, may be important in the discharging kinetics. Although injected electrons have relatively high probabilities of being captured into shallow levels, they can subsequently be emitted through thermal processes. Electrons may be recaptured and reemitted and eventually trapped stably in deep levels. Thermally activated detrapping will be particularly important in the region of space-charge-intensified field near the positive electrode. This results in the centroid of trapped charge being located closer to the silicon-oxide interface at room temperature than at liquid nitrogen temperature.

When a large positive voltage is applied to the field plate in order to field-inject electrons into the oxide, the effect of the stress time can be explained as follows: As the stress time is increased, the number of trapped electrons becomes larger, and the resulting space charge enhances the electric field near the positive electrode (field plate). This high field detraps many of the shallowly trapped electrons in this region, and the centroid of the shallowly trapped charge moves toward the silicon-oxide interface. Also, the proportion of shallowly trapped electrons to deeply trapped electrons is reduced. For

the same reason, the proportion of shallowly trapped charge is greater and its centroid is nearer the center of the oxide when the traps are populated by optically injected electrons at low field.

4.4. Determination of the Capture Cross Section and Concentration of Electron Traps in the Oxide

The charge-carrier capturing process in insulators has been extensively studied recently.[39-41] When the displacement current is not important, the characteristics of these traps can be revealed by well developed methods.[39] However, for charge storage devices such as MAOS, MNOS, MOWOS,[42-45] and ion-implanted devices, the trap concentration is so high that many of the injected charges are trapped and their contribution to the current beyond their point of trapping is only a displacement current. This must be taken into account. In the succeeding paragraphs we shall analyze the capture process.

4.4(A). Analysis

If there is an injection of electrons into the insulator, the trap capturing and emitting processes can be described by the following two equations:

(a) Continuity:

$$q \frac{\partial n_t(x,t)}{\partial t} = - \frac{\partial j(x,t)}{\partial x}, \tag{4.19}$$

where $n_t(x,t)$ is the concentration of trapped electrons at position x and time t, and $j(x,t)$ is the current density contributed by the drifting electrons.

(b) Shockley-Read Equation:[32]

$$q \frac{\partial n_t(x,t)}{\partial t} = \sigma j(x,t) \, [N_t(x) - n_t(x,t)] - e n_t(x,t) - S\sigma_p n_t(x,t), \tag{4.20}$$

where $N_t(x)$ is the trap concentration, e is the emission rate of the trapped charges (a function of electrical field, temperature and energy

depth of the traps).[46] Several mechanisms can contribute to the charge detrapping process: Field-dependent thermally activated hopping, Poole-Frenkel emission, tunneling ionization, and impact ionization. In Eq. (4.20), S is the light intensity and σ_{op} is the photoionization cross section of the trapped charges. In Eq. (4.20), we also assume that the capture cross sections for all traps with different energy levels are the same, and that the field is strong enough so that the thermal velocity can be replaced by the drift velocity.[47]

If the experiment is conducted under the condition that the emission rate and photoionization rate are relatively low in comparison with the charge capturing rate, the first-order approximation to Eq. (4.20) is

$$q \frac{\partial n_t(x,t)}{\partial t} = \sigma j(x,t) \, [N_T(x) - n_t(x,t)] . \qquad (4.21)$$

If we integrate Eq. (4.19) with respect to the variables x and t, we obtain

$$q \int_0^x n_t(x';t)dx' = - \int_0^t j(x,t')dt' + \int_0^t j(0,t')dt' . \qquad (4.22)$$

Solution of the differential equation (4.21) results in

$$n_t(x,t) = N_T(x) - N_T(x) \, e^{- \sigma/q \int_0^t j(x,t')dt'} . \qquad (4.23)$$

Combining Eqs. (4.19) and (4.21), we have

$$- \frac{\partial j(x,t)}{\partial x} = \sigma j(x,t) \, [N_T(x) - n_t(x,t)] . \qquad (4.24)$$

Solution of this equation results in:

$$j(x,t) = j(0,t) \, e^{-\sigma \int_0^x N_T(x')dx'} \, e^{\sigma \int_0^x n_t(x',t)dx'} . \qquad (4.25)$$

Define $1/q \int_0^t j \, (0,t')dt' = N_{inj}(t)$ (4.26)

Here $N_{inj}(t)$ is the number of the total particles injected into the insulator up to time t.

Substituting Eq. (4.22) into Eq. (4.25), we have:

$$e^{\sigma/q \int_0^t j(x,t')dt'} = e^{-\sigma \int_0^x N_T(x')dx'} e^{\sigma N_{inj}} + 1 - e^{-\sigma \int_0^x N_T(x')dx'} . \tag{4.27}$$

Substituting Eq. (4.27) into Eq. 4.23), we obtain

$$n_t(x,t) = \frac{N_T(x)\left[e^{\sigma N_{inj}} - 1\right]}{\left[e^{\sigma N_{inj}} - 1\right] + e^{\sigma \int_0^x N_T(x')dx'}} . \tag{4.28}$$

From Eqs. (4.25) and (4.28) we obtain

$$j(x,t) = j(0,t) \frac{e^{\sigma N_{inj}(t)}}{\left[e^{\sigma N_{inj}} - 1\right] + e^{\sigma \int_0^x N_T(x')dx'}} . \tag{4.29}$$

For an insulator with any spatial distribution of traps, Eq. (4.28) gives the concentration of trapped electrons at position x and time t in terms of the injected electrons, N_{inj}. The capture of charged particles reduces the number of particles undergoing drift. If the injected particle current at time t is j(0,t), the remaining current density, j(x,t), at position x is a function of total injected particles $N_{inj}(t)$ and the trap spatial concentration, $N_t(x)$, and is given by Eq. (4.29). Initially, the total number of injected charged particles is relatively small, and we can write

$$e^{\sigma N_{inj}(t)} \approx 1 + \sigma N_{inj}(t) .$$

Then

$$n_t(x,t) \approx N_T(x)\, e^{-\sigma \int_0^x N_T(x')dx'} \cdot \sigma N_{inj} \tag{4.30}$$

and

$$j(x,t) \tilde{\simeq} j(0,t)\, e^{-\sigma \int_0^x N_T(x')dx'} . \qquad (4.31)$$

Therefore, the displacement current is very important at the beginning. If $N_T(x)$ is uniformly distributed, both $n_t(x,t)$ and $j(x,t)$ have exponential distributions.

If the trapping is very light, then we can place $j(x,t) \tilde{\simeq} j(o,t)$ in Eq. (4.29) and obtain

$$1 \tilde{=} \frac{e^{\sigma N_{inj}(t)}}{\left[e^{\sigma N_{inj}(t)} - 1\right] + e^{\sigma \int_0^d N_T(x)dx}} . \qquad (4.32)$$

This equation can be satisfied only if

$$e^{\sigma N_{inj}(t)} >> e^{\sigma \int_0^d N_T(x)dx} - 1 . \qquad (4.33)$$

Under this condition, Eq. (4.28) simplifies to

$$n_t(x,t) \tilde{=} N_T(x) \left(1 - e^{-\sigma N_{inj}(t)}\right) . \qquad (4.34)$$

This equation has been extensively used by many investigators in analyzing trap capture cross sections. However, its applicability is restricted by the condition imposed by (4.33). If the traps are coulombic in nature, i.e., $\sigma \sim 10^{-13}$ cm^2, and assuming an oxide thickness of 1000Å and a trap concentration of $N_T \sim 10^{18}$ cm^{-3}, the condition (4.33) can not be satisfied even though the total number of the injected charge carrier is as high as $N_{inj} \sim 1 \times 10^{13}/\text{cm}^2$. In case $N_T \sim 10^{16}$ cm^3, the condition (4.33) can be satisfied for $N_{inj} \sim 1 \times 10^{13}/\text{cm}^2$. If the traps are neutral centers, i.e., $\sigma < 10^{-15}$ cm^2, and the oxide thickness is around 1000Å, the condition (4.33) is satisfied even if the trap concentration is around 10^{18} cm^{-3}. In general, Eq. (4.34) can be used to describe the trapping mechanism if the total number of injected particles is much larger than the total number of traps.

4.4(B). Estimation of Capture Cross Section and Trap Concentration in Al_2O_3

In the previous report,[8] a measurement of the trap concentration and capture cross section was described. However, owing to the existence of the substantial number of shallow traps, the thermally activated detrapping process introduced some deviation into our results. In order to avoid the thermal effect, the experiment was performed at 93°K.

The samples used in this experiment had oxide thicknesses of about 450Å and had semitransparent Al field plates (20Ω/□, ~ 100Å). The sample was first cooled down to 93°K. Then, constant bias at an average field of 1.77 MV/cm was applied to the sample until the dark current was small enough to be neglected. Photons with energy of 5.0 eV were utilized to internally photoinject electrons from the substrate into the oxide. The external current and flatband voltage shift were recorded after each 3-5 seconds of photoinjection.

As shown by the photodepopulation results quoted previously, electron traps extend throughout the bulk of the oxide. In our analysis we shall assume that the traps are uniformly distributed, i.e., $N_T(x) = N_T$, and shall further assume that all the traps have the same electron capture cross section. The emission rate of trapped charge is a function of both temperature and field strength. By performing the photoinjection at liquid nitrogen temperature and at relatively low fields, the electrons are essentially frozen into traps so that detrapping can be neglected. Another factor contributing to electron detrapping is photoionization of the traps. As was shown in Fig. 4.1, the photoionization rate of the trapped charges can be determined by the initial slope of ΔV_{FB} vs. time. This slope is very small, and so the interaction between photons and trapped charge is weak. The photoionization cross section is estimated to be of the order of 10^{-17} cm^2. Thus, the first-order capturing approximation can be applied to determine the capture cross section and spatial concentration of the traps. If $N_T(x) = N_T$, then from Eq. (4.28) we have[42,48]

$$n_t(x,t) = \frac{N_T[\exp(\sigma N_{inj}) - 1]}{[\exp(\sigma N_{inj}) - 1] + \exp(\sigma N_T x)} \qquad (4.35)$$

where N_{inj} is the number of injected electrons per unit area and is given by

$$N_{inj} = C_{ox}\Delta V_{FB}/q + Q_{ext}/q . \qquad (4.36)$$

Here Q_{ext} is the total amount of charge that flows through the external circuit during the photoinjection process. The effective trapping efficiency is defined by

$$\eta(N_{inj}) = \frac{d(C_{ox}\Delta V_{FB}/q)}{d\ N_{inj}} .$$

Thus, $$\eta(N_{inj} = 0) = 1 - [1 - \exp(-\sigma N_T d)] / \sigma N_T d . \qquad (4.37)$$

Two variables σ and N_T have to be determined. From the initial trapping efficiency, the product of σ and N_T can be determined. By adjusting the values of σ and N_T, a theoretical plot of $C_{ox}\Delta V_{FB}/q$ vs. N_{inj} could be made. This is shown in Fig. 4.8. The electron capture cross section and trap concentration are obtained by the best fit to the experimental datas, resulting in σ = 8-9 x 10^{-14} cm^2 and N_T = 6-7 x 10^{18} cm^{-3}. Our measured trap density is an order of magnitude larger than the number of negative trapped charges (10^{17} - 10^{18} cm^{-3}) measured by Mehta, Butler and Feigl[21] in their samples of Al_2O_3. Two values of the centroid of the trapped electrons are also given in Fig. 4.8. The centroid advances gradually from 150Å to 165Å during the course of the photoinjection. The initial trapping efficiency is computed to be 90%.

The magnitude of the capture cross section indicates that the traps are coulombic in nature. The trapping kinetics at lower fields has also been studied by repeating the experiment on two other capacitors. Because of the high trapping efficiency, the plot of $C_{ox}\Delta V_{FB}/q$ vs. N_{inj} was almost linear, and so more information is required in order to make the analysis. However, the product σN_t is larger than the value obtained in Fig. 4.8. This indicates the capture cross section is increased as the field strength is lowered, thus providing further evidence that the traps are coulomb-attractive centers.

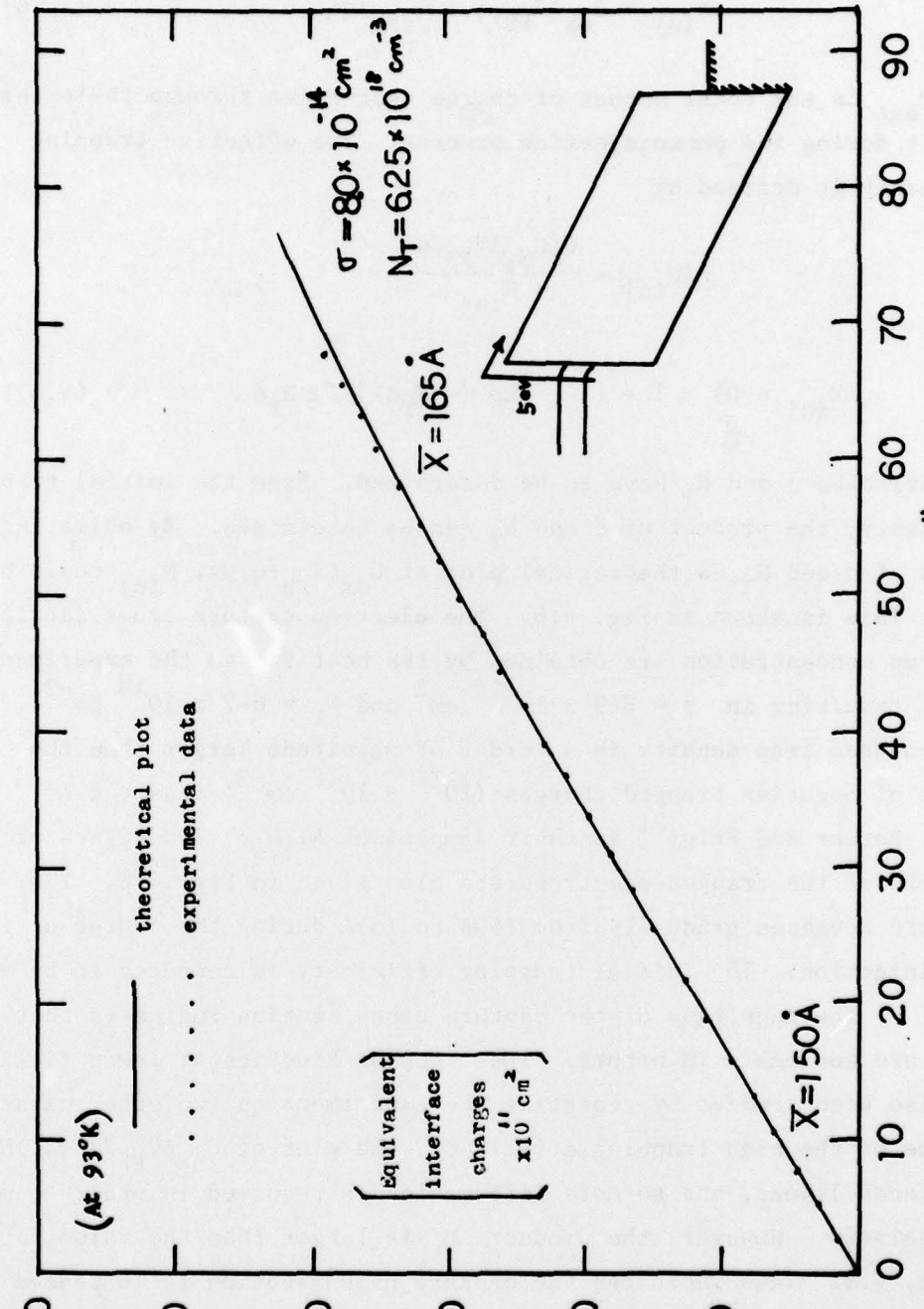

Fig. 4.8. Experimental and theoretical curves of $C_{ox}\Delta V_{FB}/q$ vs. N_{inj}.

Besides a uniform trap distribution, several special distributions frequently encountered include exponential distribution, step function distribution,[45] linear distribution, and normal distribution. By using the general equation (4.28), a similar analysis can be applied to determine the capture cross section and spatial distribution. However, more variables are involved, and so additional information is required to complete the analysis.

4.5. Effect of Thermal Annealing on the Trapping of Electrons and Holes

In this section, the charge retention ability of the device is studied at elevated temperatures. The samples used were n-substrate MAS capacitors with oxide thicknesses around 450Å. The electron traps were populated by subjecting the capacitor to an average field of 3.55 MV/cm for 2 hours. After the stressing, the flatband voltage was found to have shifted from 1.45 volts to 8.45 volts. The substrate and metal field plates were then shorted together, which caused a further reduction of flatband voltage to 6.75 volts. The discharging process here was observed to take place very rapdily, much of it occurring within 20 seconds. After 2 hours of discharging, the charge retention of the sample became quite stable.

Three samples were then annealed at three different temperatures: 70°C, 120°C, and 172°C, in vacuum for five hours each. C-V measurements were made at room temperature at various intervals, with the results shown in Fig. 4.9. The reduction of the flatband voltage takes place rapidly within the initial 60 minutes. Shallowly trapped electrons can be thermally detrapped after the temperature reaches 70°C.

Figure 4.10 shows the results of cumulative thermal treatments on two MAS structures. The sample was held at each temperature for one hour, then was taken quickly to room temperature so that the flatband voltage could be determined, after which the temperature was raised to the next higher point. Both samples show a significant change of flatband voltage between 250°C and 300°C. The estimated thermal depth corresponding to this temperature is 1.9 eV. In this estimation, the trap cross section was taken to be 1×10^{-13} cm^2. After the thermal anneal at 300°C, about 50-60% of the flatband voltage recovery is observed.

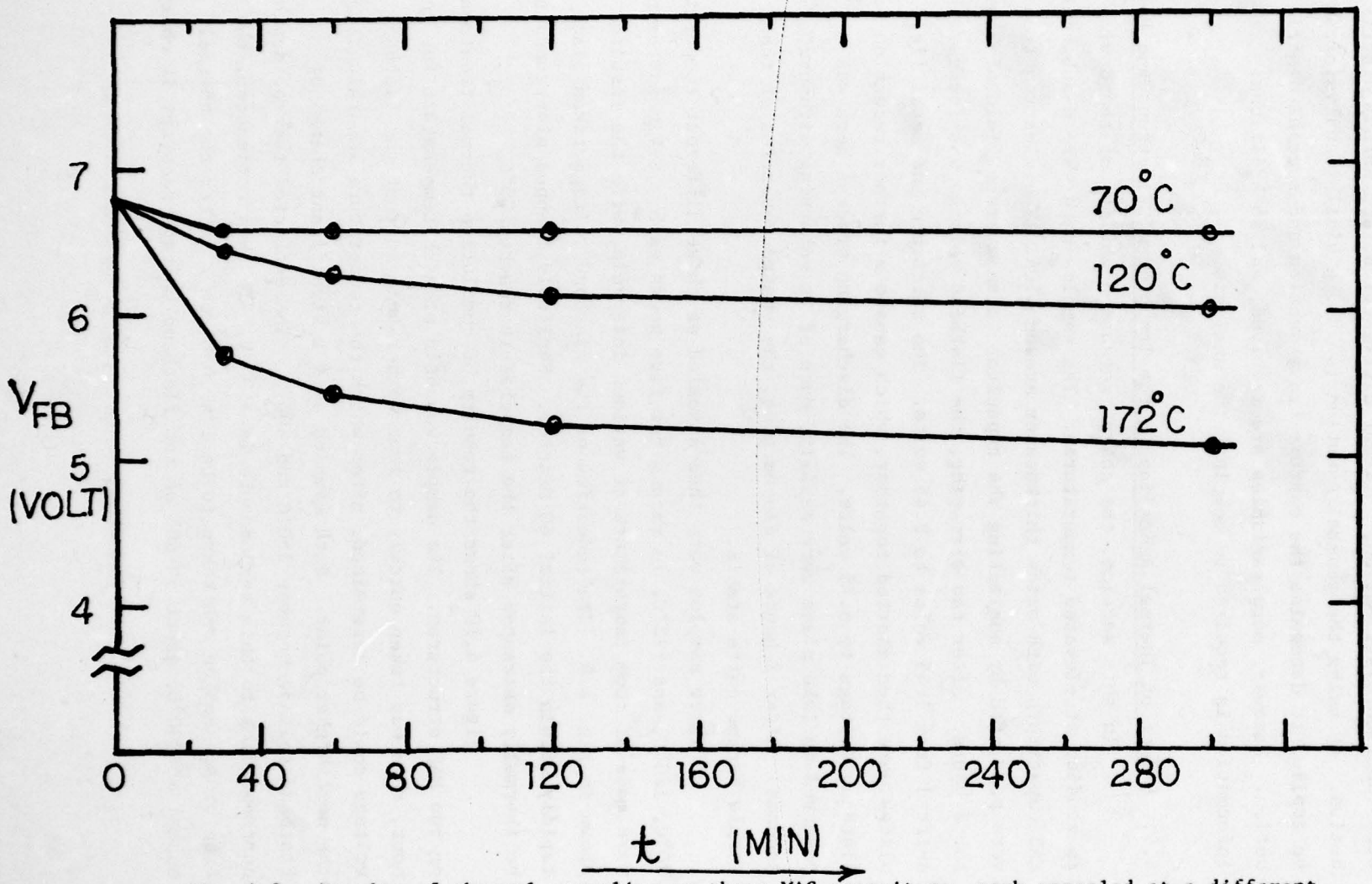

Fig. 4.9. Results of thermal annealing on three MAS capacitors, each annealed at a different temperature: 70°C, 120°C, and 172°C.

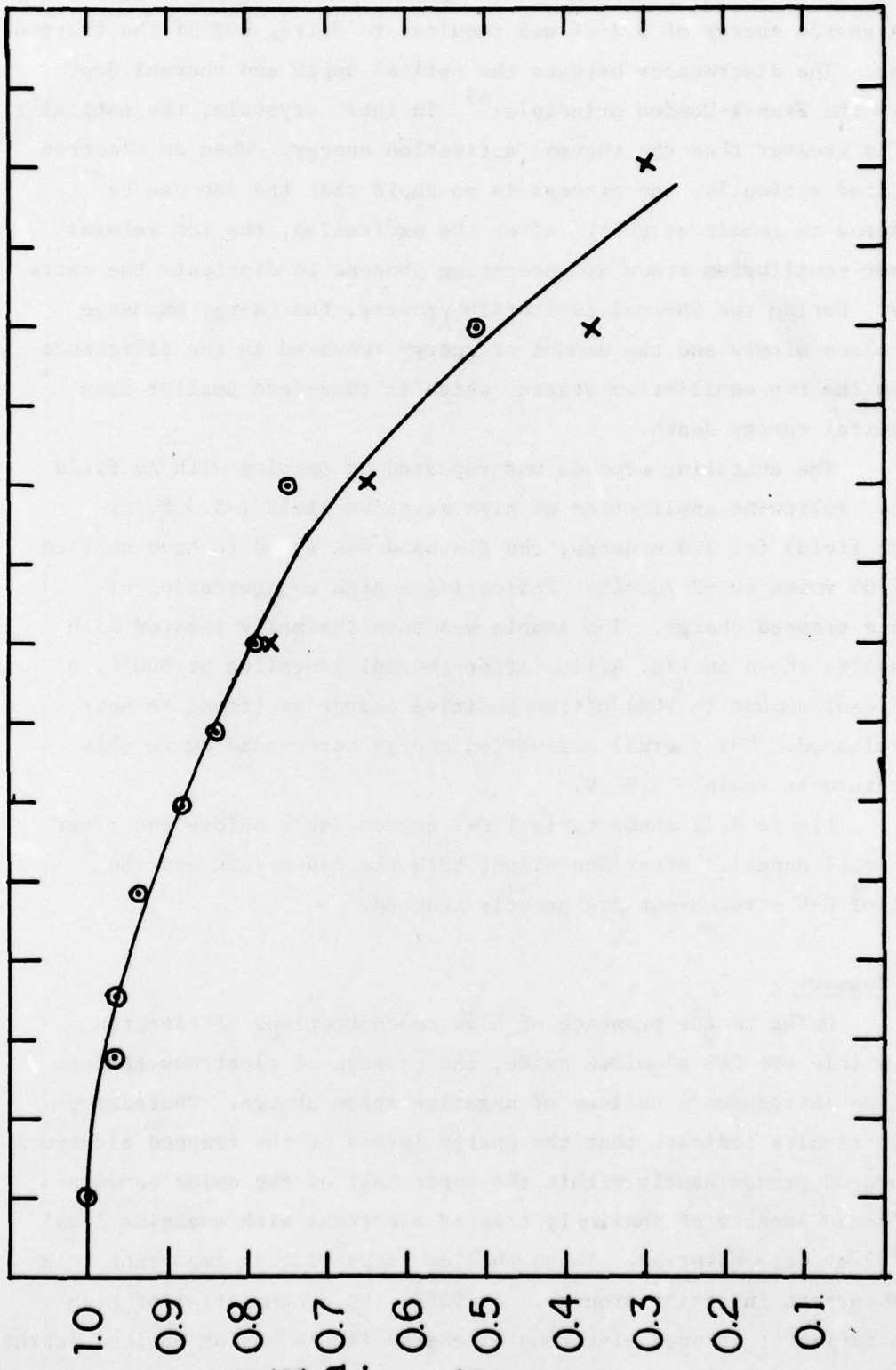

Fig. 4.10. Fraction of trapped electrons remaining in the oxide after successive thermal anneals, each step being held for one hour. The C-V measurements were made at room temperature. The curve was fitted to the data points by eye.

The studies of charge trapping by the optical bleaching technique showed that a photon energy of 3.2 eV was required to detrap 60% of the trapped charges. The discrepancy between the optical depth and thermal depth follows the Franck-Condon principle:[49] In ionic crystals, the optical depth is greater than the thermal activation energy. When an electron is excited optically, the process is so rapid that the ion can be considered to remain at rest. After the excitation, the ion relaxes to a new equilibrium state by generating phonons to dissipate the extra energy. During the thermal excitation process, the energy exchange takes place slowly and the amount of energy required is the difference between the two equilibrium states, which is therefore smaller than the optical energy depth.

The annealing process was repeated on samples with Au field plates. Following application of high negative field (-5.3 MV/cm average field) for 270 minutes, the flatband was found to have shifted from 2.05 volts to -2.7 volts, indicating a high concentration of positive trapped charge. The sample was then thermally treated with the results shown in Fig. 4.11. After thermal annealing at 300°C, a significant amount ($\sim$ 90%) of the positive charge was found to have been released. The thermal activation energy corresponding to this temperature is again $\sim$ 1.9 eV.

Figure 4.12 shows typical C-V curves taken before and after the thermal anneal. After annealing, both the hysterisis and the extent of C-V stretch-out are greatly reduced.

4.6. Summary

Owing to the presence of high concentrations of electron traps within the CVD aluminum oxide, the passage of electrons through the oxide introduces a buildup of negative space charge. Photodepopulation results indicate that the energy levels of the trapped electrons are located predominantly within the upper half of the oxide bandgap. Significant amounts of shallowly trapped electrons with energies less than 2.2 eV were observed. These shallow traps play an important role in the current injection process. At 95°K, the accumulation of high concentrations of trapped electrons at energy levels having optical depths

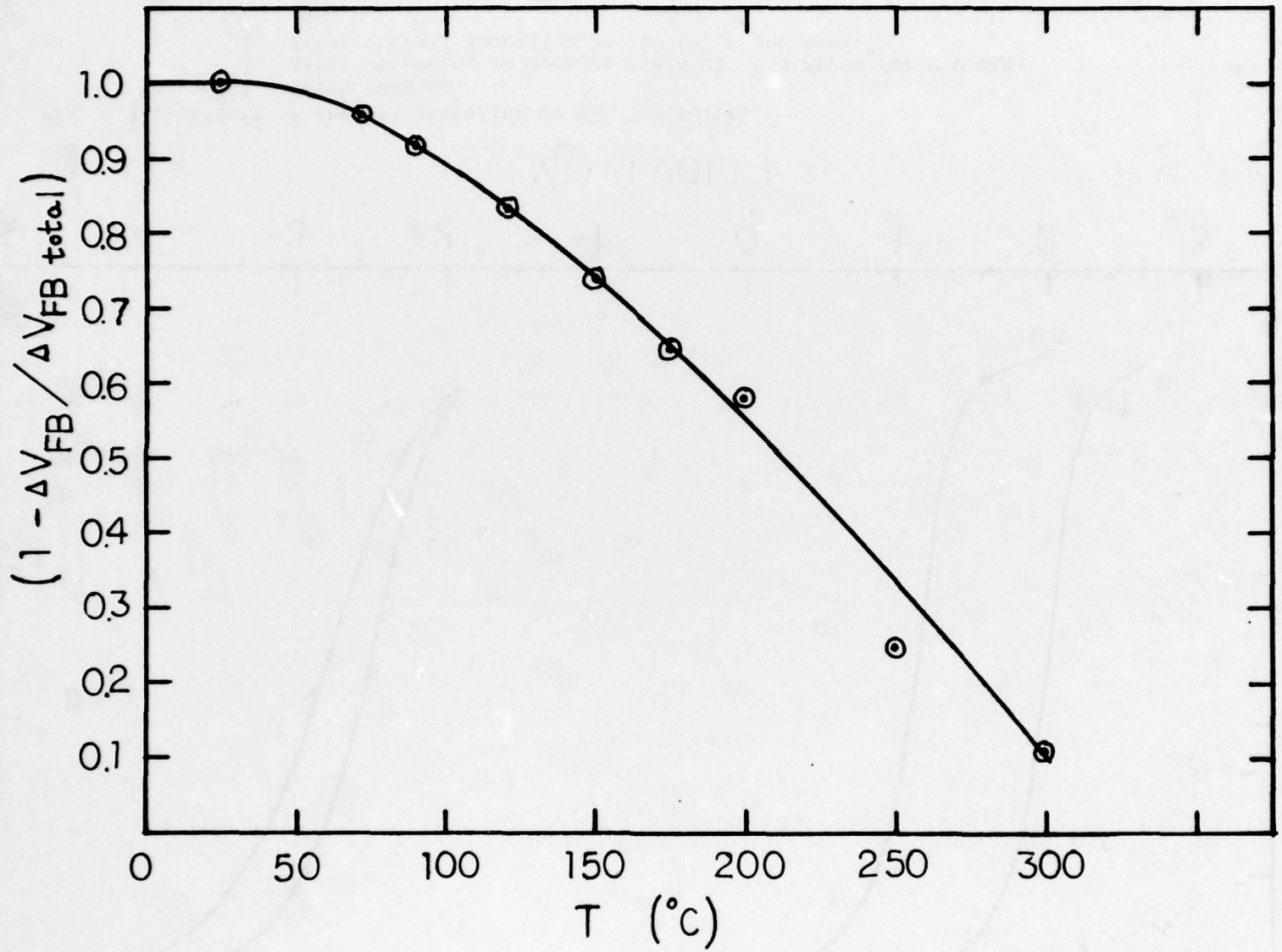

Fig. 4.11. Fraction of positive charge remaining in the oxide after successive thermal anneals, each step being held for one hour. The C-V measurements were made at room temperature. The positive charge in the oxide was the result of stressing at an average field of -5.3 MV/cm for 270 minutes. The curve was fitted by eye.

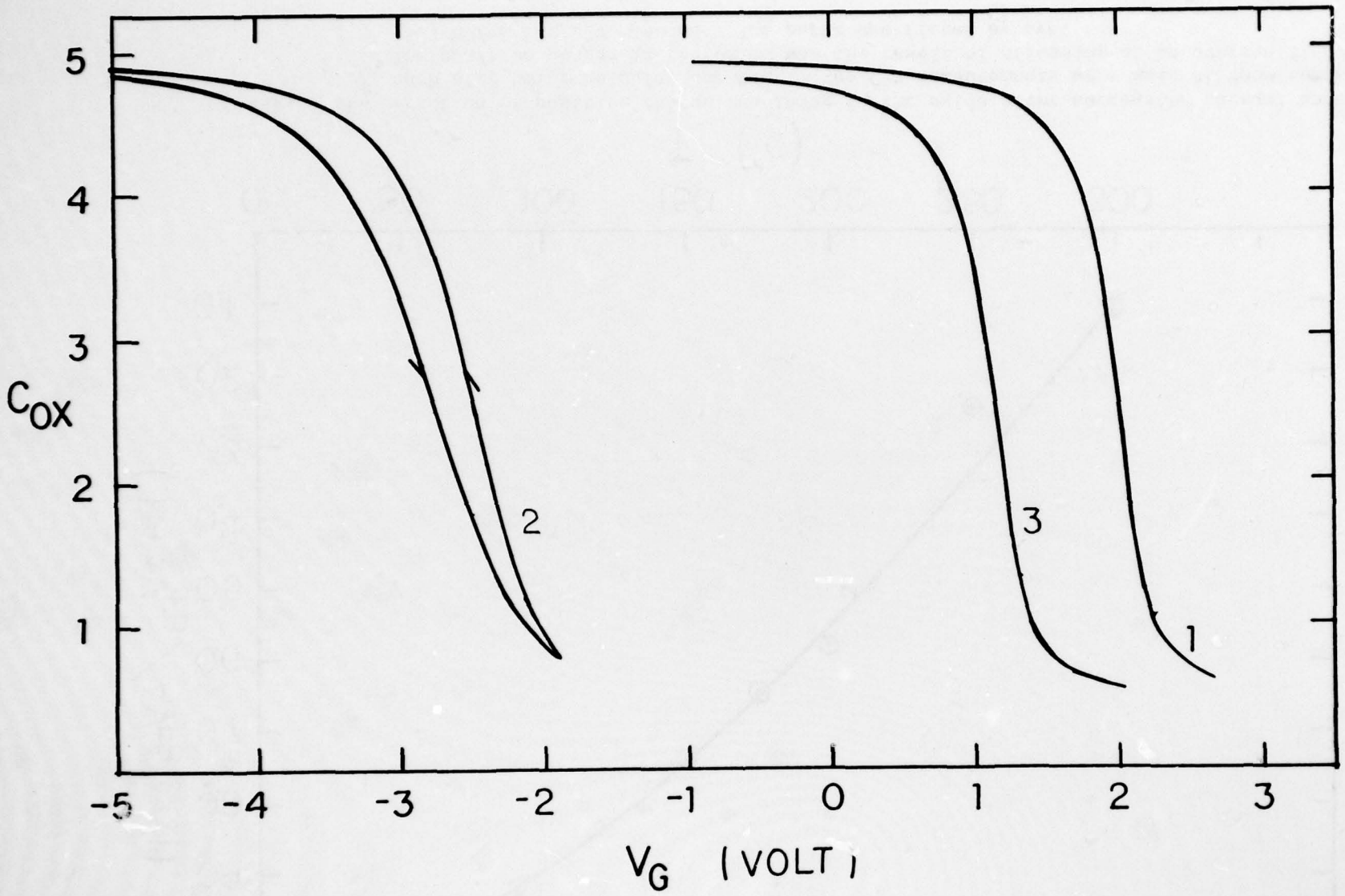

Fig. 4.12. Effect of thermal annealing on the C-V curves.
1. Fresh sample.
2. After stressing at average field of -5.3 MV/cm for 270 min.
3. After thermal annealing at 250°C for one hour.

less than 3 eV indicates either that the trap concentration is relatively high in these levels or that the capture cross section is larger than that of the deeper levels. As the temperature is increased, thermally activated detrapping processes reshape the energy profile and the spatial distribution of the trapped electrons. The major mechanisms contributing to charge detrapping are thermally-activated field-dependent hopping and Poole-Frenkel thermal emission. At room temperature, the trapped electrons tend to be concentrated in the deep energy levels and the centroid of the trapped charge is located nearer the oxide-substrate interface than at liquid nitrogen temperature. Although the injected electrons have a higher probability of being captured by shallow traps, the trapped electrons can be emitted from the shallow traps by a thermal process. The released electrons can then undergo further capture and emission, perhaps several times, before being eventually swept out of the oxide or captured into stable deep levels.

The buildup of negative space charge distorts the energy-band configuration and increases the electric field in the vicinity of the positive electrode. The detrapping rate is consequently enhanced in that region. With the field plate positive, this effect, together with the thermal activation required for detrapping, causes the centroid of the negative space charge to be located closer to the oxide-substrate interface at room temperature than at liquid nitrogen temperature.

During the course of positive-field-plate high-field stressing on an MAS structure, electrons are injected into the oxide from the substrate and many are captured by the traps. Initially, the shallow traps can capture more electrons. As the sample stressing time is increased, the thermal detrapping rate is larger than the capturing rate for the shallow traps ($E < 2.5$ eV) in the intensified field region. The total amount of shallowly trapped electrons is therefore decreased in the high field region, and the shallow electrons tend to be located in the vicinity of the oxide-substrate interface. The continuous increase of flatband voltage with time under positive bias is attributed to the electrons captured into deep levels. The measured centroid is located between 0.27 d and 0.4 d depending on the amount of shallow-level detrapping.

The characteristics of the charge trapping in charge storage devices such as MNOS has been studied extensively by others. The optical depths of the trapped electrons in these insulators is observed to be distributed from shallow levels to deep levels with energies larger than 3 eV. The study of the centroid of the trapped electrons when the traps have been populated by pulse injection indicates that the span of the charge distribution extends into the bulk of the nitride film.[42-44] The similarity between our results and the results obtained for nitride films emphasize the common characteristics of these two insulators.

For the charge storage devices, because of the high concentration of traps, the displacement current becomes extremely important. Therefore, the determination of the electron-trap capture cross section can not be done by the conventional method which assumes that the displacement current is so small that it can be neglected. We have developed a criterion which can be used to unambiguously determine whether the displacement current has to be considered in calculating the capture cross section. By taking the displacement current into consideration, we measured the capture cross section of the electron traps in CVD Al_2O_3 to be 8-9 x 10^{-14} cm^2. The magnitude indicates that the traps are coulombic in nature. The nearly neutral initial charge state of the insulator suggests that there exists compensating negative centers in the oxide. The trap concentration is as high as 6 x 10^{18} cm^{-3}; thus, the mean distance between the traps is only about 55Å, which makes it seem plausible that charge hopping can occur within this device.

REFERENCES

1. C. C. Chang, "Study of Lateral Nonuniformities and Interface States in MIS Structures," Ph.D. Dissertation, Department of Electrical Engineering. Princeton University, March 1976.

2. J. J. Clement, "A Study of Radiation Effects in MOS Capacitors", Ph.D. Dissertation, Department of Electrical Engineering & Computer Science, Princeton University, Dec. 1977.

3. Walter C. Johnson, "Study of Electronic Transport and Breakdown in Thin Insulating Filsm," Semi-Annual Technical Report No. 1 (NVL-0059-001), Contract DAAG53-73-C-0059, 1 June 1976.

4. C. S. Jenq, "High Field Generation of Interface States and Electron Traps in MOS Capacitors", Ph.D. Dissertation, Department of Electrical Engineering & Computer Science, Princeton University, Dec. 1977.

5. Walter C. Johnson, "Study of Electronic Transport and Breakdown in Thin Insulating Films," Semi-Annual Technical Report No. 2 (NVL-0059-003), Contract DAAG53-73-C-0059, 1 December 1976.

6. Walter C. Johnson, "Study of Electronic Transport and Breakdown in Thin Insulating Films," Semi-Annual Technical Report No. 3 (NVL-0059-005), Contract DAAG53-73-C-0059, 1 June 1977.

7. Walter C. Johnson, "Study of Electronic Transport and Breakdown in Thin Insulating Films," Semi-Annual Technical Report No. 4 (NVL-0059-007), Contract DAAG53-73-C-0059, 1 December 1977.

8. Walter C. Johnson, "Study of Electronic Transport and Breakdown in Thin Insulating Films," Semi-Annual Technical Report No. 5 (NVL-0059-008), Contract DAAG53-73-C-0059, 1 June 1977.

9. D. Y. Yang, W. C. Johnson, and M. A. Lampert, "A Study of the Dielectric Breakdown of SiO_2 Film on Si by Self-Quenching Technique," Special Report No. 4 (AFCRL-TR-74-0516), Oct. 1974.

10. P. S. Winokur, J. M. McGarrity and H. E. Boesch, Jr., IEEE Trans. on Nuclear Science, NS-23, 1580 (1976).

11. Kjell O. Jeppson and Christer M. Svensson, Journal of Applied Physics, 48, 2004 (1977).

12. A. G. Revesz, IEEE Trans. on Nuclear Science, NS-24, 2102 (1977).

13. C. T. Sah, IEEE Trans. on Nuclear Science, NS-23, 1563 (1976).

14. D. J. DiMaria, private communication.

15. M. Kuhn, Solid-State Electron., 13, 873 (1970).

16. R. Castagne, C. R. Acad. Sci. (Paris), B267, 866 (1968).

17. Y. T. Heow, M. R. Boudry, D. R. Lamb and S. D. Brotherton, J. Phys. D: Appl. Phys., 10, 83 (1977).

18. O. L. Curtis, Jr., J. R. Srour and K. Y. Chiu, J. Appl. Phys., 45, 4506 (1974).

19. G. A. Ausman, Jr., and F. B. McLean, Appl. Phys. Lett., 26, 173 (1975).

20. R. J. Powell and G. F. Derbenwick, IEEE Trans. on Nuclear Science, NS-18, 99 (1971).

21. D. A. Mehta, S. R. Butler and F. J. Feigl, J. Appl. Phys., 43, 4631 (1972).

22. R. J. Powell and G. W. Hughes, IEEE Trans. Nucl. Sci., NS-21, 179 (1974).

23. E. Harari and B. S. H. Royce, IEEE Trans. Nucl. Sci., NS-20, 280 (1973).

24. E. Harari, "Charge Trapping Effects in Thin Films of Al_2O_3 and SiO_2" Ph.D. Dissertation, Princeton University.

25. R. Williams, Physical Review 140, A569 (1965).

26. R. H. Walden, J. Appl. Phys. 43, 1178, (1972).

27. D. J. DiMaria and F. J. Feigl, Physical Review B, 9, 1874 (1974).

28. V. J. Kapoor, F. J. Feigl and S. R. Butler, J. Appl. Phys. 48, 739 (1977).

29. N. Szydlo and R. Poirier, J. Appl. Phys. 42, 4880 (1971).

30. D. J. DiMaria, J. Appl. Phys. 45, 5454 (1974).

31. R. J. Powell and C. N. Berglund, J. Appl. Phys. 42, 4390 (1971).

32. W. C. Johnson, "Electronic Transport in Insulating Films" IEEE Trans. Nucl. Sci. NS-19, 33 (1972).

33. D. J. DiMaria and F. J. Feigl, Phys. Review B. 11, 5023 (1975).

34. D. J. DiMaria, "The Physics of SiO_2 and its Interface", edited by T. Pantelides, Proceedings of the International Topical Conference, p. 160 (1978).

35. A. M. Goodman, Phys. Review 152, 780 (1966).

36. D. J. DiMaria, J. Appl. Phys. 47, 4073 (1976).

37. J. J. O'Dwyer, The Theory of Electrical Conduction and Breakdown in Solid Dielectrics (Oxford, 1973).

38. J. W. Gadzuk, J. Appl. Phys. 41, 286 (1970).

39. T. H. Ning and N. H. Yu, J. Appl. Phys. 45, 5373 (1974).

40. J. M. Aitken and D. R. Young, J. Appl. Phys. 47, 1196 (1976)

41. J. M. Aitken, D. R. Young and K. Pan, J. Appl. Phys. 49, 3386 (1978).

42. P. C. Arnett and B. H. Yun, Appl. Phys. Letters 26, 94 (1975).

43. B. H. Yun, Appl. Phys. Letters 25, 340 (1974).

44. K. Lehovec, J. Electronic Materials 6, 77 (1977).

45. D. R. Young, D. J. DiMaria and N. A. Bojarczuk, J. Appl. Phys., 48, 3425 (1977).

46. S. M. Sze, Physics of Semiconductor Devices (Wiley, 1969).

47. R. C. Hughes, Phys. Rev. Letters 35, 449 (1975).

48. T. H. Ning, J. Appl. Phys. 47, No. 3, 1079 (1976).

49. N. F. Mott and R. W. Gurney, Electronic Processes in Ionic Crystals (Constable and Co., 1948; Dover, 1964).